æ

16. CYTOSKELETON, CELL SHAPE, AND MOTILITY

17 December 2022

As in multicellular organisms, single cells are confronted with challenges associated with structural support and delivery of biomolecules, albeit at a different scale. Most cells rely on endoskeletons (filaments and tubules) and/or exoskeletons (cell walls) to maintain cell-shape integrity. Cell division also requires membrane-deforming proteins. In eukaryotes, various modes of internal cellular movement require cytoskeletal highways for molecular motors, which transport large cargoes using ATP hydrolysis as fuel. Central to all of these cellular features are protein fibrils and sheets comprised of long concatenations of monomeric subunits held together by noncovalent forces. How fundamental features such as cell division were carried out prior to the origin of filament-forming proteins is unknown, but the emergence of self-assembling fibrils would have been a watershed moment for evolution, providing new opportunities for cellular features requiring structural support systems.

This chapter continues an exploration of the internal anatomy and natural history of cellular components, exploring the evolutionary diversification of cytoskeletal proteins and their varied functions. The diverse sets of eukaryote-specific molecular motors and their roles in intracellular transport will also be explored. Although prokaryotes are devoid of such machines, fibrillar proteins do exist in prokaryotes, playing central but contrasting roles in structural support and cell division relative to what is seen in eukaryotes.

In eukaryotes, fibrillar proteins are also central to swimming and crawling, so this chapter will explore a few generalities with respect to cellular locomotion. Both prokaryotes and eukaryotes use flagella to swim, and such structures are sometimes suggested to be so complex as to defy an origin by normal evolutionary processes. However, not only are there plausible routes for the emergence of flagella via modifications of pre-existing cellular features, but flagella have evolved more than once. Notably, prokaryotic and eukaryotic flagella evolved independently and operate in completely different manners. Nonetheless, despite these differences, the limits to motility of single-celled organisms will be shown to follow some general scaling laws across the Tree of Life.

The Basic Cytoskeletal Infrastructure

The three major groups of fibrillar proteins will be discussed in the following sections. The two most celebrated members, actins and tubulins, are often viewed as eukaryotic innovations. However, relatives of both families have diverse functions in

various prokaryotic lineages, including cell-shape sculpting, cell division, and plasmid partitioning during replication (Ozyamak et al. 2013). This phylogenetic distribution suggests that the antecedents of both actins and tubulins were present as early as LUCA. Moreover, it bears noting that unique types of filament-forming proteins, not discussed below, are sequestered in various prokaryotic lineages (Wagstaff and Löwe 2018). This supports the idea that fibrils are not particularly difficult to evolve, the main requirements being the emergence of a heterologous interface for fibril formation from monomeric subunits and a presumed selective advantage. Indeed, for many proteins, the avoidance of mutations leading to the production of open chains is a major evolutionary challenge (Chapter 13).

Despite their sequence divergence, fibrillar proteins from very distant species faithfully assemble and function in novel host species (Horio and Oakley 1994; Osawa and Erickson 2006), indicating both a self-organizational capacity and a conserved architecture of the monomeric subunits. General reviews can be found in Wickstead and Gull (2011), Erickson (2007), Michie and Löwe (2006), and Löwe and Amos (2008). An overview of the energetic costs of producing cytoskeletal proteins in eukaryotes is provided in Foundations 16.1.

Actins. Comprised of one of the most abundant proteins within eukaryotic cells, actin polymers have diverse roles, including cell-cortex formation, vesicle trafficking, cell division, endocytosis, and amoeboid movement. Actin filaments are homopolymeric, double-stranded, and helical, ~ 7 nm in diameter (Figure 16.1). Free actin monomers are generally bound to ATP, and upon joining a filament undergo ATP hydrolysis. Actin-filament assembly is polar, with the monomeric subunits being added at the plus (barbed) end. Combined with removal at the minus end, this can result in the "apparent" movement of a filament in a treadmilling-like process (Carlier and Shekhar 2017). There are different critical concentrations of activated monomers for the plus and minus ends, and depending on the end-specific rates of addition and removal, total filament length can either grow or shrink.

Multiple actin families exist within most eukaryotes, with the variants often having different functions (e.g., Sehring et al. 2007; Joseph et al. 2008; Velle and Fritz-Laylin 2019), although yeasts and *Giardia* encode only a single copy. Numerous additional families of proteins are associated with the assembly of actin cables and networks in eukaryotes. For example, at least eight families of actin-related proteins (ARPs), related to actins by gene duplication, are involved in the nucleation of new filaments and patterning of branches off parental actins (Goodson and Hawse 2002). Profilins and formins are involved in the regulated delivery of monomers to growing filaments. WASP (Wiscott-Aldrich syndrome protein)-family proteins are involved in context-specific catalysis of ARP-induced branch growth, and appear to be essential in crawling motility (Fritz-Laylin et al. 2017). At least three major families of WASP proteins are inferred to have been present in LECA, and these have in turn diversified enormously among some phylogenetic lineages, while also being lost from others in coordination with ARP loss (Veltman and Insall 2010; Kollmar et al. 2012).

Bacterial actin-like proteins share the basic structural features of eukaryotic actin (including the contact sites at monomer interfaces and the ATP binding site involved in polymerization/depolymerization). Although this suggests phylogenetic

relatedness (Ghoshdastider et al. 2015), the sequences of eukaryotic and prokaryotic actins are substantially different (sometimes to the point of not being recognizable by this means; Bork et al. 1992), leaving the issue unresolved. Actin-like proteins with diverse functions are sporadically distributed over the bacterial phylogeny, usually with only one or two types per species. For example, MreB is involved in the maintenance of shape in rod-shaped cells, forming helical shapes around the cell periphery (Margolin 2009). ParR acts like a eukaryotic centromeric-binding protein, elongating and pushing plasmid copies to the opposite ends of the dividing parental cell using an actin-like concatamer of ParM (Salje et al. 2010). In some bacteria, magnetite crystals organize along a MamK filament, creating a magnet used in orientation (Bazylinski and Frankel 2004). Expression of DivB in punctate foci during times of stress induces *Streptomyces* to grow into branching, filamentous mats.

Although usually consisting of double-stranded helices, these broad families of bacterial filaments vary widely with respect to the periodicity of twists and even the direction of helix winding (handedness). A protein harbored by the archaeon *Pyrobaculum calidifontis,* crenactin, has close sequence similarity to eukaryotic actins and again shares similar helical structure (Ettema et al. 2011; Braun et al. 2015; Izoré et al. 2016). All of these observations strongly suggest that an actin-like protein was present in LUCA.

Tubulins. The second major group of eukaryotic fibrils is comprised of tubules, which assemble through the stepwise addition of heterodimers of α- and β-tubulin subunits. Typically, 13 protofilaments are assembled into hollow cylindrical microtubules, approximately 25 nm in diameter (Figure 16.1), $\sim 2.5\times$ that of actin filaments. Unlike actins, which depend on ATP hydrolysis for assembly, tubulins use GTP hydrolysis. Like actin filaments, microtubules are polar in nature. The minus ends are generally anchored at a microtubule-organizing center, such as a centrosome, a spindle-pole body, or a basal body. Growth and contraction occurs at the opposite end in a process known as dynamic instability, which plays a central role in various aspects of cell motility (Mitchison and Kirchner 1984; Gardner et al. 2013; Akhmanova and Steinmetz 2015).

As with actins, there is clear evidence that the antecedents of tubulins were present in LUCA, the most telling of which is FtsZ, a bacterial protein that assembles into homomeric filaments that can form bundles (but not organized microtubules). Despite having very low sequence identity, FtsZ subunits are nearly identical in structure to tubulin monomers, and the few sites conserved between FtsZ and tubulin are almost all involved in GTP binding (Löwe and Amos 2009). FtsZ produces rings that guide bacterial cell division, although at least one bacterial group (the Planctomycetes) deploys an unrelated protein for such purposes (Van Niftrik et al. 2009). Notably, FtsZ-related proteins are also present in numerous eukaryotes, where they form the division ring responsible for fission of mitochondria and chloroplasts. This is presumably a vestige of these organelles having arisen by bacterial endosymbiosis (Chapter 23), although the loss of such proteins from a number of eukaryotic lineages (including metazoans) implies alternative modes of organelle division (Kiefel et al. 2004; Bernander and Ettema 2010).

α- and β-tubulin are products of an ancient, pre-LUCA gene duplication. In

addition to these two types, at least six other distinct tubulin families are known in eukaryotes (although only γ seems to be present in all lineages), and these are generally deployed in different cellular constructs, e.g., basal bodies out of which cilia and flagella grow, rails for vesicle transport, and mitotic/meiotic spindles used for chromosome separation. Such diversification of function is sometimes called the multi-tubulin hypothesis (McKean et al. 2001; Dutcher 2003). Divergent variants even exist within the α and β subtypes. Consider, for example, two closely related amoeboid protists with extreme forms of pseudopodia. Foraminiferans produce branching networks (reticulopodia) that assist in prey capture, whereas radiolarians produce stiff, spine-like structures (axopodia) that assist in floating and capturing prey. Each group deploys a uniquely modified β tubulin to construct the helical filaments involved in such structures (Hou et al. 2013).

Tubulins can also assemble into higher-order structures. For example, most eukaryotes harbor a pair of barrel-shaped organelles called centrioles, comprised largely of microtubules. With few exceptions, centrioles consist of rings of nine microtubule triplets, with the overall structure resembling a cartwheel. Throughout eukaryotes, centrioles serve as the basal body from which flagella and cilia grow (below). Phylogenetic analysis implies their presence in the ancestral eukaryote, with losses in a few lineages, including yeasts and land plants (Carvalho-Santos et al. 2010, 2011; Hodges et al. 2010).

In animals and some fungi, centrioles have a second role, assembling into centrosomes that serve as the organizing center from which the mitotic spindle expands during cell division (Chapter 10). Some insects have evolved centrioles with much more elaborate structures than the conventional nine-triplet cartwheel, whereas a few protists have simpler structures (Gönczy 2012). The mechanisms driving such change remain unknown. During sexual reproduction in animals, the centriole is excluded from the egg and introduced via the sperm, possibly an evolutionary outcome of sexual conflict and/or sperm competition driving the high rate of evolution of centriolar protein sequences (Carvalho-Santos et al. 2011; Ross and Normark 2015).

Although the 13-protofilament microtubule appears to be unique to eukaryotes, variants of this form exist in some prokaryotes. For example, some members of the Verrucomicrobiales genus *Prosthecobacter* contain two tubulin-like genes, BtubA and BtubB, that form heterodimers, which in turn polymerize into four-filament microtubules capable of dynamic instability and are also joined by a third protein seemingly related to a eukaryotic motor protein (Pilhofer et al. 2011; Deng et al. 2017). The emergent picture is that FtsZ and the tubulins are all members of a common family of proteins, with Btub possibly having arisen by horizontal transfer from a eukaryote and evolving a heterodimeric form after gene duplication.

One of the more interesting aspects of actin and tubulin-related proteins is their exchanged roles in cell division in eukaryotes vs. prokaryotes. As noted above, cytokinesis involves a tubulin-like (FtsZ) ring in bacteria but an actin ring in eukaryotes. In contrast, whereas microtubules are universally used to move chromosomes apart in eukaryotes, actin-like molecules are involved in the partitioning of plasmid genomes in most bacteria (Larsen et al. 2007; Salje et al. 2010; Szewczak-Harris and Löwe 2018), although tubulin-like molecules are used in still others (Larsen et al. 2007). This differential utilization of fibrillar proteins provides a clear example

of convergent evolution of the same function from substantially different starting points. Notably, phylogenetic subgroups of the archaea also appear to deploy diverse sets of filaments in cytokinesis, some FtsZ-like and others actin-like (Lindås et al. 2008; Samson and Bell 2009; Makarova et al. 2010; Pelve et al. 2011).

Finally, as will be noted below, eukaryotic actins and tubulins act in consortia with motor proteins to accomplish a wide array of intracellular functions. However, fibrils are also capable of work on their own, creating pushing forces that can be used to move various organelles and to deform the cell membrane. How can this occur if the fibrils grow at the tips that are in contact with their targets? Although not all of the details are worked out, it appears that continued fibril elongation occurs by a sort of Brownian motion ratchet (Mogilner and Oster 1996). Slight fluctuations at points of contact allow occasional room for a new monomer to join the pushing end of the fibril, thereby ratcheting the point of contact forward.

Intermediate filaments. A third group of fibril forming proteins known as intermediate filaments are structurally quite unlike tubulins and actins, forming unpolarized cables and sheets that are not dynamic. Although such structures are ultimately assembled from dimeric subunits, unlike the situation in actins and tubulins, these organize into coiled coils before further development into higher-order structures (Figure 16.1). Intermediate filaments are mostly confined to metazoans and slime molds, where they have a variety of functions involved in structural support, e.g., lamins, keratins, and desmins (Preisner et al. 2018). This restricted distribution, sequestered to one clade, suggests a post-LECA origin. However, a potential homolog, crescentin, determines cell shape in the bacterium *Caulobacter crescentus.*

Cell Shape

Cells come in a wide variety of sizes and shapes. Indeed, unicellular eukaryotes often have such characteristic shapes that they are often used as diagnostics for identification to the genus or species levels, e.g., as in diatoms and dinoflagellates. Bacteria also have a wide range of possible cell shapes (Young 2006), although only a small number of these are commonly utilized. Most bacteria are either spherical or rod-shaped with an average axial (length:width) ratio of ~ 3, with nonmotile cells being spheres more frequently than are flagellated cells (Dusenbery 1998; Young 2006). When confined to constricted settings or forced to bend, bacteria can mold into novel shapes, but upon release to more natural settings, they return to their characteristic shapes (Männik et al. 2009; Amir et al. 2014), demonstrating both a capacity for plasticity and a significant degree of genetic determinism. Cytoskeletal fibrils and cell walls provide support structures essential for maintaining shape.

The main challenge from an evolutionary perspective is understanding the selective pressures that promote the maintenance of particular shapes in specific ecological contexts. Although the evolutionary advantages of alternative cell shapes are unknown in most cases, a variety of factors have been envisioned (Pirie 1973; Marshall 2011; Pančić et al. 2019). For example, given the known behavior of different shapes within fluids, e.g., spheres, oblate spheroids (flat ellipsoids), and prolate

spheroids (elongate ellipsoids), the advantages of alternative forms can be postulated from a purely biophysical perspective (Dusenbery 1998; Schuech et al. 2019). If there is a premium on increased surface area (as would be the case if cell surface area limited nutrient uptake), disk-shaped cells would be expected to be common. However, such forms are almost never found among bacteria (one exception being *Haloquadratum,* which forms flat squares), although some diatoms have them. Spheres (which have a minimum surface:volume ratio) have the highest rate of diffusion through a liquid, and would be selectively promoted if random dispersal (with no direct motility) were to be advantageous. On the other hand, the sedimentation rate of spheres exceeds that of all other ellipsoids, which may be disadvantageous under many conditions, e.g., phytoplankton sinking out of the photic zone. Up to a $2.4\times$ reduction in sinking rate occurs with a rod-like form, but this maximum effect requires an axial ratio of ~ 30, far beyond what is typically observed (some needle-shaped diatoms being an exception). Swimming efficiency is greatest for a rod with an axial ratio of 2 (Dusenbery 1998), which minimizes drag, but this relative length is smaller than what is typically seen.

Why then are rod-shaped bacteria so common? Rods may be advantageous in environments where sheer forces are high, as they are able to attach to solid surfaces better than spheres. Environmental sensing (Chapter 22) may also be enhanced in elongate cells, which can have a 100 to 600-fold enhanced capacity to sense the direction of chemical gradients (Dusenbery 1998). This can be accomplished by simultaneously sensing the environment at both ends of the cell or by performing a temporal survey by swimming across environmental gradients. Spheres are much more subject to rotational diffusion (and hence loss of directionality) than rods.

Despite the uncertainties regarding ecological selective forces, rod-shaped bacterial cells appear to follow specific scaling patterns. Rods generally grow only in length (not width), and this keeps the surface area:volume roughly constant over the cell cycle, as the end caps make only a small contribution. The surface area:volume (SA:V) ratio is maintained near $2\pi V^{-1/3}$, at both the level of individual species when grown under different nutritional levels as well as at the phylogenetic (between-species) level (Ojkic et al. 2019). In both cases, the relative surface area increases as cell volume declines. This specific SA:V scaling is accomplished by maintaining the aspect ratio (length:width) at a constant value $\simeq 4$. Under this scaling pattern, as a cell doubles in volume, the SA:V ratio decreases by a factor of 1.26.

Although the specific underlying selective forces are not always clear, cellular dimensions can be responsive to relatively simple modifications at the molecular level. The molecular toolbox for cell-shape determination in bacteria primarily involves two cytoskeletal molecules noted above: the tubulin-like FtsZ and the actin-like MreB. For rod-shaped cells, MreB and its relatives direct the synthesis of the sidewalls in ways that ensure uniform width (Margolin 2009; Typas et al. 2011; Ursell et al. 2014; Dion et al. 2019). On time scales of just a few years, laboratory cultures of *E. coli* have been found to evolve increases in cell volume via a single mutation in the MreB gene. Additional studies show that substitutions of the 20 alternative amino acids at just one amino-acid site in the MreB gene generate a range of cell sizes, with an increase in growth rate accompanying an increase in cell volume up to a point (Monds et al. 2014). Numerous other examples exist in which simple manipulations of the protein-coding regions of MreB and FtsZ elicit radical

shifts in cell form, e.g., spheres to rods to long filaments (Young 2010).

When MreB is deleted entirely, rod-shaped cells generally shift to more spherical forms (Margolin 2009), and indeed bacteria that are naturally coccoid have invariably lost MreB. However, some rod-shaped bacteria have also lost MreB, implying the presence of alternative methods for the maintenance of this shape. Moreover, even when MreB is utilized in the formation of the same cell shape in different species, the end point can be achieved by rather different mechanisms. For example, the two model bacteria, *E. coli* and *B. subtilis,* use MreB to maintain their rod shapes, but the helical movement of this molecule proceeds in a left-hand fashion in the former and a right-hand fashion in the latter. In addition, the deployment of MreB in wall growth differs. *E. coli* regulates the amount of peptidoglycan loaded per MreB patch, whereas *B. subtilis* regulates the speed of growth of individual MreB patches (Wang et al. 2012). The two species also differ in the ways in which they integrate subunits into the cell wall, the thickness of which in *E. coli* is only $\sim 10\%$ that in *B. subtilis* (Billaudeau et al. 2017).

Lactococcus lactis lacks MreB and is typically an ovoid cell, but under certain environmental conditions the cells can become rod-shaped, even extending to long filaments. FtsZ is involved in these transformations (Pérez-Núñez et al. 2011). As noted above, this protein generally directs the production of the cross-wall septum during cell division, but in *L. lactis* multiple rings of the division proteins develop along the filaments, inhibiting complete septation. This kind of transition from spherical (coccoid) to rod-shaped cells has been seen in other bacteria (Lleo et al. 1990), but cases are also known in which shifts from rod to coccoid shapes are elicited by deletions of genes other than FtsZ and MreB (Veyrier et al. 2015). Thus, although it has been suggested that the ancestral bacterium was rod-shaped (Siefert and Fox 1998; Tamames et al. 2001), with coccoid forms being derived evolutionary dead-end states, the ease of both transitions leaves little room for such a simple interpretation.

Cell Walls

Most prokaryotes maintain their cell shapes via external cell-wall structures. The same is true for fungi, green plants, and many other lineages of unicellular algae. In addition to their roles in cell-shape determination, such outer coverings can have other functions, such as protection against pathogens and consumers. Structural support also allows freshwater cells to resist the turgor pressure that inevitably results from high intracellular molarity, which encourages the influx of water molecules from the environment (Chapter 18). Cells lacking such pressure resistance would blow up without active mechanisms for the continuous efflux of water. Raven (1982) makes the point that cell walls represent a one-time investment against the osmolarity problem, whereas an active mechanism of water removal, e.g., a contractile vacuole, incurs costs that must be paid throughout the life of the cell. Assuming negligible costs of cell-wall maintenance, the latter expense must eventually surpass the former in slower-growing cells.

Bacteria. One of the most striking variants of cell-wall architecture distinguishes Gram-negative from Gram-positive bacteria (originally identified by a difference in staining intensity of the cells). Bacterial cell walls are constructed primarily out of peptidoglycan (often called murein), which consists of a mesh of polysaccharide (glycan) chains linked together by short peptides (Figure 16.2). Gram-positive bacteria (also known as monoderms) have a single cell membrane surrounded by a thick cell wall, whereas Gram-negative bacteria (diderms) sandwich a thin peptidoglycan layer between two lipid membranes (often with an additional layer of lipopolysaccharides on the cell surface). Although the basic structure of peptidoglycan is universal, there is substantial variation among bacterial lineages with respect to peptide sequence, location of crosslinks between the peptide chains, and secondary modifications of the components (Vollmer and Seligman 2010).

How a dual-membrane form could have evolved from an ancestor with a single membrane (assuming this was, in fact, the ancestral bacterial state) is an unsolved problem. One idea derives from the observation that monoderms often produce double-membrane endospores. These are produced by engulfment within the maternal cell, with the plasma membrane of the mother becoming an external membrane of the spore (Vollmer 2011; Tocheva et al. 2016). Some diderm bacteria can also produce endospores wherein the outer membrane of the maternal cell is displaced by the inner membrane (Tocheva et al. 2011). These observations show how a cell can undergo special kinds of divisions to establish an altered cell envelope. However, such changes are terminal and lost upon spore germination, so such repatterning is a far cry from demonstrating how a stable developmental pattern of two-layer biogenesis is acquired in an evolutionary sense. One interpretation of extant bacterial phylogeny is that the ancestral bacterium was a sporulating diderm (with monoderms losing the outer membrane) (Tocheva et al. 2016). If correct, this would be another example of the regression of complexity to simpler forms (while still leaving the origin of the diderm phenotype unexplained).

Like Gram-positive bacteria, archaea nearly always have single lipid membranes, often surrounded by a variant of peptidoglycan (pseudomurein) and then by an outer crystalline shell called the S layer (Albers and Meyer 2011; Visweswaran et al. 2011; Oger and Cario 2013). S layers consist of highly organized, essentially crystalline protein lattices, with substantial variation in design among species. As there is significant variation in the biosynthetic pathways leading to murein (bacteria) and pseudomurein (archaea), and little homology between the genes involved, it has been suggested that the cell walls of these two groups evolved independently (Hartmann and König 1990; Steenbakkers et al. 2006).

Although cell walls provide obvious advantages in many ecological settings, they have been lost in a few bacterial lineages (e.g., *Mycoplasma* and *Ureaplasma*). Numerous eukaryotic lineages do not have cell walls, and it remains unclear as to whether LECA did. Multiple lines of evidence suggest that cell walls comprise a substantial fraction of a cell's energy budget, imposing a use-it-or-lose situation, i.e., a strong advantage to loss during prolonged periods in which the investment in biosynthesis outweighed the fitness advantages. The energetic costs of wall construction can be made for the well-understood bacterium *E. coli* in the following way (Lynch and Trickovic 2020), using methods developed in Chapter 17.

The carbohydrate subunit of peptidoglycan consists of two joined molecules,

NAG (N-acetylglucosamine) and NAM (N-acetylmuramic acid), with short peptide chains fused to the latter for cross-bridging. The total cost of synthesis of each peptidoglycan unit can be shown to be $\sim$ 209 ATP hydrolyses, and there are $\sim 3.5 \times 10^6$ disaccharides in the entire cell wall (Wientjes et al. 1991; Gumbart et al. 2014), implying a total cost of $\sim 7.3 \times 10^8$ ATP hydrolyses (which constitutes $\sim 2.7\%$ of the total cell-growth budget). The *E. coli* envelope also contains $\sim 10^6$ molecules of Braun's lipoprotein (Li et al. 2014; Asmar and Collet 2018), which attach the outer membrane to the cell wall. Each of these molecules consists of a chain of 58 amino acids (worth $\sim$ 34 ATPs each, including chain elongation) and three chains of palmitate ($\sim$ 122 ATPs each) for a total cost of $(58 \times 34) + (3 \times 122) = 2338$ ATPs per unit, implying $\sim 2.3 \times 10^9$ ATPs in total, or $\sim 8.5\%$ of the total cell budget. There are in addition $\sim 1.2 \times 10^6$ lipopolysaccharide molecules on the surface of the cell (Neidhardt et al. 1990), with a cost of 1048 ATPs per molecule, accounting for another 3.6% of the cell's construction budget. Finally, the total cost of lipids in the cell membranes of *E. coli* comprises $\sim 34\%$ of the cell budget (Chapter 17). Thus, summing all of these components, the entire envelope constitutes $\sim 49\%$ of the energy budget of an *E. coli* cell. This is likely a downwardly biased estimate, as the costs of surface antigens attached to the ends of lipopolysaccharides (and present in variable amounts in different strains) have been ignored.

Extension of this sort of analysis to the Gram-positive bacterium *B. subtilis* leads to the conclusion that, despite substantial envelope organization differences relative to *E. coli,* about a third of the total-cell energy budget is allocated to the envelope (Lynch and Trickovic 2020). Thus, for species with cell walls, lipid membranes are generally still the most expensive components of the envelope. Most significantly, the overall cost of the bacterial cell envelope constitutes a larger fraction of a cell's energy budget than any other single component, although this declines with increasing cell volume as a consequence of the reduction in surface area:volume ratio (Chapter 17).

Eukaryotes. Numerous wall types exist in eukaryotes. One macro-scale classification uses categories related to whether walls are internal or external to membranes, neither, or both (Becker 2000), although such a scheme belies the underlying diversity in chemical makeup (Niklas 2004). For example, structural support in diatoms is provided by silicious shells. The thecal plates of dinoflagellates, and the scales of haptophytes, chrysophytic algae, and other phytoplankton species are constructed from diverse substrates, including calcite, chitin, and cellulose (Okuda 2002).

One of the most common constituents of eukaryotic cell walls, possibly the most abundant biomolecule in the world, is a linear polymer of glucose residues called cellulose. Found throughout plants, some slime molds, some bacteria, and even a group of animals (tunicates), this simple molecule has variants among phylogenetic lineages, with the glucose residues sometimes carrying modified side chains. The phylogenetic distribution of cellulose biosynthetic capacity, along with the conserved structure and sequence of the underlying machinery, strongly suggests its movement into and throughout eukaryotes by horizontal transfer events. The ultimate agent may have been the endosymbiotic colonist that formed the chloroplast. However, it remains a mystery as to why eukaryotes have completely abandoned the use of peptidoglycans, if they ever had them. Notably, biosynthesis of peptidoglycan

in bacteria starts with UDP-acetyl glucosamine (where UDP denotes uridine diphosphate), whereas cellulose biosynthesis starts with UDP-glucose, implying either an ancient common ancestry for the production of such building blocks, or another case of convergent evolution.

Contrary to the situation with bacterial peptidoglycan, which is held together by peptide cross-linking, cellulose consists of long aggregated filaments of the underlying glucose derivatives held together by intra- and inter-chain hydrogen bonds. Cellulose production proceeds in a spatially organized fashion via large, membrane-bound cellulose synthase complexes, organized in rows, arrays, or rosettes that define the variable dimensions of the resultant microfibrils and their mesh-like forms in different species (Niklas 2004; Saxena and Brown 2005). However, in seemingly no case do eukaryotic cell walls consist solely of cellulose, with a wide variety of glycoproteins, lignins, pectins, uronic acids, xyloglucans, and many other subunits being utilized in various forms of cross-linking in individual lineages (Niklas 2004; Domozych et al. 2014). In the brown algae, cellulose is a relatively minor component of cell walls, the majority consisting of other forms of linked polysaccharides called alginates and sulfated fucans, both thought to have been acquired by horizontal transfer from bacteria (Michel et al. 2010).

Even rough estimates of the costs of these components would be useful. Using methods outlined in Chapter 17, based on the known biosynthetic pathway, the cost of each glucan subunit of cellulose is equivalent to ~ 34 ATP hydrolyses, although the total investment that cells make in cellulose (which requires estimates of the total number of subunits per wall) remains an open question. Deposition of silicon into the frustules of diatoms may be relatively cheap, involving the expenditure of perhaps just a single ATP per incorporated molecule, with the total cost to a cell being only $\sim 2\%$ of the total energy budget (Raven 1983), although this ignores the underlying organic wall components.

Explicit insight into the substantial costs of walls can be achieved for the well-studied budding yeast by considering the following numbers. Yin et al. (2007) estimate that $\sim 21\%$ of the biomass of a *S. cerevisiae* cell consists of the cell wall ($\sim 4\%$ protein, 30% mannose, 60% glucan, and 1% chitin). The glucan subunits are derived from $\sim 7.7 \times 10^9$ glucose molecules, which would otherwise be available for cellular energy or as carbon skeletons for other biosynthetic pathways, and the $\sim 1.7 \times 10^6$ protein molecules per adult cell surface constitute $\sim 2\%$ of the total protein content of the cell (Klis et al. 2014). Similar numbers were obtained for another yeast species, *Candida albicans* (Klis et al. 2014).

Given these observations, a rough estimate of the cost of the cell wall in *S. cerevisiae* can be calculated as follows. Mannose is a simple derivative of glucose and comprises half the biomass of the glucans, so together these two constituents account for the equivalent of $\sim 1.5 \times 7.7 \times 10^9 = 1.2 \times 10^{10}$ glucose molecules. Noting that *S. cerevisiae* has an average cell volume $\simeq 70\ \mu\text{m}^3$, Equation 8.2b implies that the cost of building a yeast cell $\simeq 1.6 \times 10^{12}$ ATP hydrolyses. Assuming that a glucose molecule is equivalent to 32 ATPs under aerobic respiration (Chapter 17), this translates to a cost of 5×10^{10} in units of glucose molecules. Thus, mannose and glucans together account for $\sim 26\%$ of the energetic growth requirements in this species. Assuming an average cost of synthesizing and concatenating amino acids of ~ 34 ATP hydrolyses each (Chapter 17), and an average protein length of 400 amino

acids, the cost of wall proteins $\simeq 1.7 \times 10^6 \times 400 \times 34 = 23 \times 10^9$ ATPs, which is $\sim 1.4\%$ of the total energy budget. With the cell membrane in this species constituting an additional 4.6% of the cell budget (Chapter 17), the entire cell envelope in *S. cerevisiae* comprises $\sim 32\%$ of the total cell energy budget.

Molecular Motors

In prokaryotes, most intracellular molecular transport is passively driven by random diffusion resulting from background thermally induced molecular motion. In contrast, a good deal of molecular movement in eukaryotes involves active transport, which comes at a cost. Actins and tubulins can exert mechanical pressure on their own, as they push against larger structures and thermal fluctuations allow the stochastic insertion of monomeric subunits and progressive extension. However, molecular-motor proteins supplement the cytomotive capacity of the cytoskeletal filaments, using them as highways for dragging along attached cargoes (Figure 16.3). Such motors transduce chemical energy into mechanical force via ATP hydrolysis, engaging in diverse functions, ranging from cargo transport to the movement of flagella (Howard 2001).

Given their apparent absence from prokaryotes, all three major families of cytoskeleton-associated motors – dynein, kinesin, and myosin – likely emerged on the path between FECA and LECA. Myosins travel exclusively on actin filaments, whereas kinesins and dyneins operate on microtubules (tubulin filaments). Although their physical structures vary, each type of molecule works by the same mechanism. Each motor molecule has an ATP-binding site, a track-binding site, and a tail domain involved in cargo attachment. Some details remain unclear (Hwang and Karplus 2019), but the molecules effectively walk along their cytoskeletal roadways, with each ATP hydrolysis resulting in one step forward (in some cases two hydrolyses occur per step; Zhang et al. 2015).

Ubiquitous to all eukaryotes, kinesins underwent massive diversification into an estimated eleven families prior to LECA (Lawrence et al. 2004; Wickstead et al. 2010). Prominent roles include vesicle transport, spindle assembly, chromosome segregation, and intraflagellar transport of flagellar components. Monomeric, dimeric, trimeric, and tetrameric forms exist, and the multimers may be either homomeric or heteromeric. The motor domains generally operate like walking feet paired together at one end of the molecular structure, although tetramers have motor domains on both ends. Kinesin movement is generally unidirectional, towards the + ends of microtubules (usually moving from the center to the edges of cells), with typical rates of movement on the order of 0.5 to 1 μm/sec and stride lengths $\simeq 8$ nm (Block et al. 1990; Howard 2001; Muthukrishnan et al. 2009; Scholey 2013). Those involved in meiosis and mitosis are much slower, with speeds on the order of 0.05 μm/sec. Different kinesins vary in neck lengths, and these and other molecular features determine the degree of processivity of the motors along tubulin filaments (Hariharan and Hancock 2009; Shastry and Hancock 2010; Cochran 2015).

Myosins are nearly ubiquitous among eukaryotes, but apparently have been lost from the red algal, diplomonad, and trichomonad lineages (Richards and Cavalier-

Smith 2005; Foth et al. 2006). Although myosins and kinesins differ in size and exhibit little sequence similarity, given the similar 3-D structures of their functional domains, they may have evolved from a common ancestor (Kull et al. 1998). The most likely ancestral state prior to eukaryotic diversification is something on the order of three myosin classes, all derived from a single common ancestral protein en route from FECA to LECA. However, like kinesins, myosins further diversified into a large number of subclasses (as many as 24; Foth et al. 2006; Goodson and Dawson 2006), again with numerous functions, including cellular motility, and transport of organelles, vesicles, and mRNAs. An argument has been made that diversification of myosin functions followed paths of subfunctionalization, from generalized to more specialized forms (Mast et al. 2012).

Although most myosins are dimeric with parallel coiled-coil domains, monomeric forms exist, as do dimers with anti-parallel constructs with actin-binding domains at each end (Quintero and Yengo 2012). Almost all myosins move in the + direction of actin filaments. Each type of molecule has a specific affinity for certain types of filaments, a particular step length (usually 5 to 40 nm per step), and speeds often in the range of 0.3 to 0.5 μm/sec (Elting et al. 2011). However, a myosin involved in cytoplasmic streaming in plant cells can move at rates up to 60 μm/sec (Titus 2016). Exceptionally high rates occur when myosins run rather than walk, jumping from point to point with actual step lengths greater than those that can be accomplished when one motor domain is always in contact with the filament.

The third major class of motor proteins, dyneins, has a substantially different structure than kinesins and myosins, including an intramolecular hexameric ring consisting of AAA (ATPases Associated with cellular Activities) domains, all physically linked in a single gene (Kardon and Vale 2009). Containing > 4500 amino-acid residues, dyneins are among the largest known proteins. In total, there are at least nine deeply diverging dynein lineages, most of which trace back to LECA, although they were independently lost in the lineages leading to land plants and red algae. Dyneins maintain the attribute of having two walking feet, with each step fueled by ATP hydrolysis. However, contrary to the situation with kinesins and myosins, dyneins always walk towards the $-$ ends of microtubules, typically towards the cell center, and with variable speeds in the range of those noted above (Walter and Diez 2012; Sweeney and Holzbaur 2016). Dyneins are also unique in that all but one cytoplasmic family member is associated with the cilium (Wickstead and Gull 2007; Wilkes et al. 2008). The latter operate in a team-like fashion to cause microtubules to slide past each other, thereby eliciting ciliary movement.

Although molecular motors have been subject to numerous biochemical and biophysical studies, few questions have been asked from an evolutionary perspective. The three central phenotypic features of motor proteins are their step length, step rate, and processivity (distance progressed before falling off a substrate). All three parameters are readily estimated in laboratory constructs, and the rate of movement is equal to the product of the length and rate of steps, but almost nothing is known about how these traits vary among species or among motor family members within species. In addition, the total drain on a cell's energy budget owing to motor activity is essentially unknown.

Motility

All cells are capable of movement, even if simply as a consequence of the physical forces associated with cell division. Here, however, our concern is with active movement within the lifespan of a cell, as in swimming or crawling. The range of cellular motility mechanisms is diverse, and Miyata et al. (2020) catalog 18 distinct modes of single-cell movement. Moreover, even seemingly similar, complex structural features such as flagella have evolved independently in different lineages. Regardless of the mechanism, all forms of motility require an investment of energy, either a gradient of hydrogen ions driving a turbine-like apparatus or active hydrolysis of ATP used in the conversion of chemical to mechanical energy for flagellar flexing. In addition, the construction of the motility machinery itself can require a substantial energetic investment. Thus, unless active motility provides a boost in fitness, the mechanism will be liable to rapid loss, as this can free up substantial energy for other cellular functions.

The details of how simple cells can utilize sensory mechanisms to direct motion will be addressed in Chapter 18. The primary focus here is on the evolutionary origins of motility machineries and the costs of building and running them. Flagella and cilia have received considerably more attention than mechanisms of crawling, and accordingly are given the most attention in the following sections. A broad overview of bacterial motility systems is given in Wadhwa and Berg (2022).

Crawling. Numerous bacteria are capable of movement on solid surfaces (Jarrell and McBride 2008; Nan and Zusman 2016; Wadhwa and Berg 2022). For example, some bacteria, such as *Neisseria,* can crawl over surfaces by twitching of Type IV pili, whereas members of the Bacteroidetes glide by use of surface adhesins, and still others move by an inchworm-like mechanism involving membrane-embedded proteins. In addition, crawling is achieved by similar enough molecular mechanisms over diverse phylogenetic groups of eukaryotes that it has been argued that LECA was capable of such movement (Fritz-Laylin et al. 2017). Thus, given that a similar conclusion has been reached on the origins of the eukaryotic flagellum (below), and the fact that numerous eukaryotic lineages have cells capable of both flagellar swimming and amoeboid movement (Fulton 1977; Brunet et al. 2021; Prostak et al. 2021), LECA may have been capable of both forms of motility.

Despite the approximate uniformity of crawling mechanisms in eukaryotes, most notably the shared use of actins and actin-associated proteins to generate expansion and retraction of cellular protrusions, a variety of structures are used. These can generally be classified into two major groups: 1) pseudopods, which involve broad protrusions underlain by branched actin-networks that allow cells to drag themselves across surfaces; and 2) filopods, which involve narrower, linear extensions of unbranched actin bundles that enable a more walking-like motion. Unlike more permanent flagella, all such structures are dynamic, allowing rapid changes in shape via local assembly and disassembly of the underlying cytoskeleton. One of the primary side activities associated with crawling is the ingestion of food particles by phagocytosis.

In general, crawling on surfaces proceeds at much lower speeds than swimming

through liquids. For example, the amoeba *Naegleria gruberi* crawls at a rate of 1 to 2 μm/sec (Preston and King 2003, which is one to two orders of magnitude lower than typical swimming speeds for prokaryotes and eukaryotes of similar size (below). Gliding motility in *Myxococcus* is even slower, on the order of 0.03 μm/sec (Tchoufag et al. 2019).

Little is known about the energetic cost of crawling in unicellular species. However, based on the cost of actin polymerization, Flamholz et al. (2014) estimated that the crawling motion in a goldfish keratocyte (cells that normally colonize the cornea in vertebrates) consumes $\sim 4 \times 10^5$ ATPs/second. Recalling from Chapter 8 that the basal metabolic requirement of a vertebrate cell $\simeq 5 \times 10^7$ ATPs/second, and that, assuming a one-day cell division time, the cost of building such a cell is $\sim 6 \times 10^8$ ATPs/second, the cost of crawling in this particular case is on the order of 1% of such a cell's operational budget (and $\sim 0.1\%$ of the total energy budget).

Prokaryotic flagella. Some planktonic cyanobacteria, such as *Synechococcus,* can swim without flagella (Waterbury et al. 1985), and others are capable of buoyancy regulation via gas vacuoles (Walsby 1994), but the vast majority of bacterial movement in open water involves a flagellum, one of the most complex molecular machines within bacterial cells (Figure 16.4). The dozens of proteins contributing to overall flagellar structure can be divided into five major components: the basal body (which includes the membrane-embedded stator within which the motor rotates); the switch; the hook; the filament; and the export apparatus. Bacterial flagellar assembly starts at the basal body, anchoring the overall structure to the cell membrane, and then proceeds to the construction of the hook, and finally to the filament. The latter is a hollow, tubular structure, consisting of tens of thousands of flagellin molecules, making this one of the most abundant proteins in swimming bacterial cells. Its assembly proceeds by the export of flagellin proteins through the central pore. Specific chaperones are assigned to each exported protein, which have to remain unfolded while in transit to the tip. The monomeric flagellin subunits are then configured into helical forms, which vary in structural arrangements both within and between species (Turner et al. 2000; Kreutzberger et al. 2022).

Unicellular species live in a low Reynold's number world (Foundations 16.2), where viscous forces dominate to such a degree that there is essentially no inertia upon cessation of activity. Thus, bacterial flagella essentially operate like cork screws, pulling the cell forward through an effectively syrup-like environment. Generally driven by a proton-motive force (but in some species, by a sodium-motive force or even by divalent cations; Ito and Takahashi 2017), the helical filament rotates within the membrane-embedded hub (Manson et al. 1977, 1980; Meister et al. 1987). The overall structure is reminiscent of a rotor guided by a surrounding stationary stator in an electrical motor, although the primary flagellar motor is run by series of still smaller motors (Figure 16.5). As the protons pass through channels, the associated rotational force is applied to the internal shaft, analogous to the coordinated pairing of gears associated with a bicycle chain. Speed and orientation can be regulated through various signal transduction systems that modify flagellar activity (Wadhams and Armitage 2004; Boehm et al. 2010; Chapter 22).

Despite the intricacies of the bacterial flagellum, there is substantial phylogenetic variation in its basic features, including the angularity and periodicity of the

helices, clockwise vs. counter-clockwise rotation, the number of distinct flagellin proteins incorporated into the filament, and the number of protofilaments per flagellum (Pallen and Matzke 2006; Galkin et al. 2008; Chaban et al. 2018; Kaplan et al. 2019). Variation also exists in the structure and number of components in the basal body and in the cellular positions and numbers of flagella (Chen et al. 2011; Moon et al. 2016; Chaban et al. 2018; Rossmann and Beeby 2018). Although the flagella of most bacteria are not surrounded by membranes, they are present in numerous genera including *Helicobacter, Vibrio,* and *Bdellovibrio* (Seidler and Starr 1968; Geis et al. 1993; Zhu et al. 2017). In spirochaetes, the flagella are not even external, but reside within the periplasmic space (between the two membranes), where their twisting contorts the entire cell. The degree to which the scattered presence of flagella throughout the bacterial phylogeny is due to lineage-specific losses or gains by horizontal gene transfer remains unclear (Snyder et al. 2009).

How might a molecular machine as complex as a bacterial flagellum have arisen? Paths of descent with modification of pre-existing structures are supported by several lines of evidence. For example, the subcomponent that drives flagellar component export appears to be related to the catalytic subunits of ATP synthase. In addition, the remainder of the system appears to be related to cell-surface projections used to transfer infection-determining proteins into host cells, so-called Type-III secretion systems (Pallen et al. 2005). At least ten components of such secretion systems have strong homologies to components of the bacterial flagellum, and the overall architecture is similar. The main difference is that the secretion system harbors a stiff injection apparatus rather than a flagellum (Blocker et al. 2003; Egelman 2010).

Liu and Ochman (2007) provide evidence that least 24 of the > 50 genes whose products comprise the bacterial flagellar system were likely present in the common ancestor to all bacteria, and that many of the components were derived by gene duplication. They further suggest that the order of inferred duplications imply an "inside-out" sequence of evolutionary steps that in turn reflects the assembly process, i.e., from basal body to hook to junction to filament, a potential example of ontogeny recapitulating phylogeny. These observations suggest that the flagellum arose from something like a Type-III secretion system, rather than the other way around, although this is not an iron-clad conclusion. Just as the flagellum may have evolved from bacterial structures with alternative functions, partial loss of the flagellum sometimes leads to the maintenance of structures with novel functions. For example, *Buchnera aphidicola,* an endosymbiont that inhabits the cells of aphids, has lost the flagellar filament, but the cells still harbor hundreds of hook/basal body structures, with likely roles in secretion into host cells, much like Type-III secretion systems (Maezawa et al. 2006; Toft and Fares 2008).

Finally, although fairly similar in overall structure, the flagella of archaea appear to be completely unrelated to those of bacteria, providing a remarkable example of convergent evolution (Kreutzberger et al. 2022). As in bacteria, the archaeal flagellum (often called the archaellum) rotates via an embedded membrane structure. However, rather than being driven by a proton-motive force, ATP hydrolysis directly drives rotation of the archaellum (Thomas et al. 2001; Desmond et al. 2007; Lassak et al. 2012; Daum et al. 2017; Albers and Jarrell 2018). The components of the archaeal flagellum appear to be unrelated to bacterial flagellins, and unlike the situation in bacteria, archaeal flagella are not hollow, have no hook structure,

and appear most closely related to bacterial type IV pilus systems (Albers and Pohlschröder 2009), which are used as adhesive structures and in twitching motility, although this too might be a matter of convergence.

Eukaryotic flagella. This theme of diversity extends to the eukaryotic flagellum, which differs from anything utilized in the prokaryotic world. Unlike the rotational flagella of prokaryotes, eukaryotic flagella operate by a whip-like mechanism driven by ATP-consuming motor proteins, which cause doublets of microtubules to slide past each other. Only a few eukaryotic lineages lack the ability to produce flagella, most notably slime molds, yeasts, and land plants, motivating the conclusion that the origin of the eukaryotic flagellum preceded LECA (Cavalier-Smith 2002; Nevers et al. 2017). In some protists, such as ciliates and parabasalids, enormous proliferations of short flagella coat large portions of the cell surface. The word cilia (singular cilium) is generally reserved for these cases, although aside from length differences relative to cell size, the basic structure remains the same.

Eukaryotic flagella are much larger than those in bacteria, generally on the order of 200 nm in diameter as compared to 10 to 30 nm in prokaryotes. They almost always consist of rings of nine peripheral microtubule doublets surrounding a central pair (Ginger et al. 2008; Ishikawa and Marshall 2011, 2017). This overall core structure, known as an axoneme, is surrounded by an extension of the cell membrane. The doublets grow out of cylinders known as basal bodies, which consist of triplets of δ- and ϵ-tubulins that arose by gene duplication prior to LECA (Dutcher 2003). In most eukaryotes, the basal bodies are recycled centrioles, which are used as mitotic-spindle organizing centers during cell division.

While bacterial flagella are comprised of a few dozen distinct proteins, on the order of 250 to 500 proteins contribute to the eukaryotic flagellum, up to 3% of the proteins encoded in a eukaryotic genome (Avidor-Reiss et al. 2004; Pazour et al. 2005; Smith et al. 2005). For the few organisms for which the flagellar proteome has been evaluated (the green alga *Chlamydomonas,* the ciliate *Tetrahymena,* and mammals), ~ 200 proteins are flagellar-specific and not found in nonciliated species (Avidor-Reiss et al. 2004; Smith et al. 2005).

Numerous activities occur within the lumens of eukaryotic flagella. As there are no ribosomes within the flagellum, all materials must be selectively imported by intraflagellar transport (IFT). Eukaryotic flagella also contain metabolic machinery for generating ATPs to fuel the molecular motors involved in transport and motility (Ginger et al. 2008). Kinesins move structural components forward on one member of each microtubule doublet, while dyneins move cargo in the opposite direction on the other member, preventing bi-directional traffic collisions (Stepanek and Pigino 2016). Transport rates are on the order of 1 to 3 μm/sec (Ishikawa and Marshall 2017).

The most convincing hypothesis for the evolution of the eukaryotic flagellum invokes an autogenous origin, starting as protruding microtubule bundle emanating from a microtubule organizing center (as used in mitotic spindles) (Cavalier-Smith 1978; Jékely and Arendt 2006). The initial structure may have had little to do with motility at all, operating instead as an environmental sensing organ. Indeed, flagella also function secondarily as sense organs, harboring numerous signal-transduction systems (environmental sensors that initiate information cas-

cades within cells; Chapter 22). The central pair of microtubules is typically absent in derived structures called primary cilia, which are used as sensing organs in cells of metazoa.

Eventually an IFT system would have to evolve, along with the ninefold symmetric structure of the axoneme, and the recruitment of molecular motors. Such a scenario may have involved little more than a series of gene duplication and modification events associated with the tubulins and motor proteins deployed in the cellular interior (Hartman and Smith 2009). An alternative hypothesis postulates an origin via a virus that somehow convinced a host cell to produce a primitive basal body for extruding viral particles (Satir et al. 2007; Alliegro and Satir 2009). An obvious problem with this idea is its failure to address the cost of maintaining such a harmful pathogen for the eons required for the emergence of the complex ciliary structure.

Further insight into the origins of the components of the eukaryotic flagellum derives from similarities to various features of the nuclear pore complex and vesicle scaffolding proteins. Fibers at the base of the flagellum may operate as gateways to admission of appropriate protein cargoes for intraflagellar transport, making use of RAN-GTP cycles and importin molecules as in the case of transport through nuclear pores (Rosenbaum and Witman 2002; Dishinger et al. 2010; Kee et al. 2012). Notably, the two IFT protein complexes that bind to cargoes (and are in turn dragged by motors) appear to have arisen by duplication from a common ancestor related to vesicle-coat proteins (van Dam et al. 2013). As noted in Chapter 15, the latter proteins are in turn related to the scaffold of the nuclear pore complex. Left unresolved here is whether the nuclear-pore complex preceded the evolution of the flagellum or vice versa, but these observations again illustrate how the complex features of cells often evolve by duplication and modification of pre-existing structures rather than by *de novo* establishment.

As in bacteria, there are many variants on the structure and deployment of eukaryotic flagella. For example, the green alga *Chlamydomonas* can swim either by a breaststroke or by undulatory waves (Tam and Hosoi 2011). The cryptophyte *Ochromonas* has perpendicular hairs (mastigonemes) radiating from the flagellum, creating a feather-like appearance. Combined with the use of flagella, euglenoids are capable of additional cell contortions (called metaboly), shifting the positions of cellular contents progressively along its axis like food moving through an animal's gut (Noselli et al. 2019). In trypanosomes, a single flagellum is embedded along the side of the cell.

The eukaryotic flagellum has served as a model for understanding how size homeostasis is maintained for cellular organelles, one of the key questions in developmental biology focused at the cellular level (Chapter 9). Inappropriate flagellum lengths (including unequal lengths in species with paired flagella) lead to aberrant swimming patterns (Tam et al. 2003; Khona et al. 2013). Because eukaryotic flagella undergo constant assembly and disassembly of tubulin subunits (Marshall and Rosenbaum 2001), maintenance of a constant length and symmetry implies that the two rates must be balanced. This further requires that at least one of the two reaction rates be length-dependent, such that the rate of disassembly exceeds that of assembly above the equilibrium length, and vice versa below the equilibrium. Such regulation is supported by experiments in the biflagellated *Chlamydomonas,*

showing that when one flagellum is severed, it grows back while the other shrinks until the two equilibrate in length (Ludington et al. 2012, 2013). The data appear to support an active-disassembly model, with depolymerization increasing with flagellum length (Fai et al. 2019), and this is also true for *Giardia,* which has four pairs of flagella of different lengths (McInally et al. 2019).

The costs of swimming. Although many cells can swim, and it is easy to imagine adaptive reasons for doing so, e.g., directive movement towards patchy resources and avoidance of predators, not all cells living in aquatic environments can self-propel. The latter include many planktonic bacteria, diatoms, and green algae. This suggests that the energetic cost of swimming in certain settings may exceed the benefits. Drawing from prior work (Lynch and Trickovic 2020; Schavemaker and Lynch 2022), rough estimates are now provided for the costs for both the act of swimming and of building the mobility apparatus.

The minimum power requirement for swimming can be estimated as the work required to move an object (usually assumed to be a sphere, or an alternatively shaped cell suitably transformed to an effective sphere) at a particular velocity (Foundations 16.2). In biology, however, the mechanical force essential for movement is obtained from chemical energy, i.e., ATP hydrolysis. As this is a less than perfect conversion process, the ultimate cost must exceed the expectations based on mechanical energy alone. From comparisons of the cost predictions of physical theory with the actual costs of moving flagella, the universal conclusion from a diversity of organisms is that the conversion of chemical energy into motion is quite low: $\sim 0.1\%$ for the ciliate *Paramecium* (Katsu-Kimura et al. 2009); 1.3% for the euglenoid *Eutreptiella* (Arroyo et al. 2012); 0.8%, 1.5%, and 1.4%, respectively, for the green algae *Chlamydomonas* (Tam and Hosoi 2011), *Polytoma uvella* (Gittleson and Noble 1973) and *Tetraflagellochloris mauritanica* (Barsanti et al. 2016); 8% for the archaeon *Halobacterium* (Kinosita et al. 2016); and 1% and 5%, respectively, for the bacteria *E. coli* (Purcell 1977; Chattopadhyay et al. 2006) and *Streptococcus* (Meister et al. 1987). Thus, the power requirement for swimming is on the order of $100\times$ that expected based solely on the physics of the process. Brownian-motion jostling of cells, rotational diffusion, helical swimming patterns, and flexibility of the flagellum are among the reasons for this low efficiency.

Despite these low efficiencies, it has been suggested that the total cost of swimming is trivially small (Purcell 1977). However, this sort of statement needs context, especially from an evolutionary perspective. Only a few attempts have been made to estimate the cost of swimming, but Raven and Richardson (1984) concluded that the cost of running a flagellum for an idealized dinoflagellate is about equal to the basal metabolic rate, whereas Katsu-Kimura et al. (2009) suggested 70% for the ciliate *Paramecium.* Crawford (1992) estimated that 1 to 10% of ciliate and dinoflagellate *total* energy budgets are allocated to swimming, whereas Fenchel and Finlay (1983) estimated fractional total cellular costs of $\sim 0.4\%$ in the cryptomonad *Ochromonas* and the ciliate *Didinium.* These quantitative differences in results are not necessarily incompatible, as metabolic rates are generally just a small fraction of total cellular energy budgets.

Although fractional energy investments as low as 0.1 to 1% may seem trivial in an absolute sense, such costs can easily be perceived by natural selection in most

populations. As discussed in Chapters 4 and 5, the power of selection is almost always sufficient to perceive a cost as low as 0.01% (and orders of magnitude lower in unicellular species). Thus, the cost of swimming is sufficiently large that such a trait exists in an evolutionary "use it or lose it" context. That is, the promotion of nonmotile mutants is highly likely if the benefits of motility do not exceed the costs.

There are, however, a number of uncertainties in this broad range of estimates, and a more general view of the problem can be obtained from the phylogenetic scaling relationship between swimming velocity (v in units of μm/sec) and cell volume (V in units of μm^3) (Figure 16.5a). For eukaryotic species, average $v \simeq 17V^{0.25}$, and noting that the radius of a sphere is $r = (3V/4\pi)^{1/3}$, this suggests a swimming speed for unicellular eukaryotes of $\sim 13V^{-0.08}$/sec in units of effective cell diameters ($2r$). The average estimates are then near 4 and 13 lengths/sec, respectively, for the largest ($V = 10^6$) and smallest ($V = 1$) swimming cells of eukaryotes. Some ciliates are capable of "jumping" behavior, which yields rates of 130 to 150 lengths/sec (Gilbert 1994). For bacteria, average swimming speeds in units of cell length are even more extreme: scaling as $\sim 24V^{-0.16}$/sec, or 17 and 35 lengths/sec for the largest ($V = 10$) and smallest ($V = 0.1$) bacterial cells.

Scaled by organismal length, swimming speeds for eukaryotic cells are comparable to those observed for the larvae of marine invertebrates, which generally fall in the range of 5 to 10 lengths/sec (Chia et al. 1984), and much higher than those for swimming vertebrates (fish, birds, seals, and whales), nearly all of which fall in the range of 0.5 to 2.5 m/sec (Sato et al. 2007). The peak speeds of the fastest fish (marlins and sailfish) are $\sim$ 15 body lengths/sec, and the maximum speed for an Olympic swimmer is $\sim$ 2 body lengths/sec. Despite their small size and simplicity, bacteria are clear champions of the swimming world.

How much energy does such activity demand? From Equation 16.2.2, it can be seen that the power required for swimming scales with the product of the viscosity of the medium (η), the radius of the cell (r), and the squared swimming velocity (v^2), and to account for the inefficient conversion from chemical energy to motion, this must further be multiplied by 100 (from above). Assuming spherical cells, the scaling relationship for eukaryotes in Figure 16.4a implies $rv^2 \simeq 171V^{0.83}$ μm^3/sec^2. From Chapter 3, the viscosity of water is 10^{-2} g $\cdot$ cm^{-1} $\cdot$ sec^{-1} (assuming 20°C), and after applying this to Equation 16.2.2 and appropriate changes of units, the average power requirement of swimming is estimated to be $(1.6 \times 10^{-16})V^{0.83}$ kg $\cdot$ m^2 $\cdot$ sec^{-3}, which has equivalent units of joules/sec (here, cell volume V is in units of μm^3).

To put this in more familiar terms, note that a rough estimate of the energy associated with the hydrolysis of one mole of ATP at physiological conditions is 50 kilojoules. After allowing for Avogadro's number of molecules per mole, the power requirement for swimming in units of ATP molecules hydrolyzed/hour is then $\sim (17 \times 10^6)V^{0.83}$ for eukaryotic cells, and similar extrapolation leads to $(54 \times 10^6)V^{0.67}$ for bacteria. Recalling that average basal metabolic rates scale isometrically with cell volume, $\simeq 0.4 \times 10^9 V$ ATP hydrolyses/hour at 20° C (Chapter 8), this suggests a fractional energetic investment in swimming (relative to total maintenance costs, and assuming the cell is constantly swimming) in the range of 1 to 4% for the largest and smallest eukaryotic cells, but substantially higher in bacteria, ranging from 6% in the largest to 29% in the smallest swimming species.

Notably, these estimates do not include the cost of building the swimming ap-

paratus. As outlined in Foundations 16.3, the total biosynthetic cost of the proteins comprising each *E. coli* flagellum and its basal protein parts is equivalent to $\sim 10^8$ ATP hydrolyses. Recalling from Chapter 8 that the total cost of building an *E. coli* cell is $\sim 2.7 \times 10^{10}$ ATP hydrolyses, the bioenergetic cost of building each of the multiple flagella is then on the order of 0.4% of the total cellular energy budget. The flagella of some bacteria are surrounded by a lipid membrane, and although *E. coli* is not one of them, were it to do so, the additional cost would be $\sim 3.6 \times 10^8$ ATP hydrolyses per flagellum, raising the total construction cost by $\sim 5\times$ relative to that for a naked flagellum. Recalling from above that the cost of swimming is $\sim (54 \times 10^6) V^{0.67}$ ATP hydrolyses per hour for bacteria, because the average volume of an *E. coli* cell is $V \simeq 1$ μm^3, the cell-division time is typically no more than a few hours, and an average cell harbors several flagella, more than 50% of the cost of swimming will typically be associated with building as opposed to operating the apparatus. There will, of course, be quantitative differences among species after variation in flagellar lengths and numbers and cell size are accounted for. However, a larger analysis of ~ 40 bacterial species reveals that the absolute costs of flagellar construction scale isometrically with cell volume, with a median cost of $\sim 4\%$ relative to total cell construction costs (Figure 16.5b,c).

Calculations for eukaryotes (Foundations 16.3) suggest roughly similar relative costs of swimming. Noting that the volume of a *C. reinhardtii* cell is ~ 150 μm^3, and allowing for a 24-hour cell division time implies an energetic cost of swimming of $\sim 2.6 \times 10^{10}$ ATP per cell life time, whereas the costs of flagellar construction are $\sim 3 \times 10^{10}$ ATP hydrolyses for the protein content and $\sim 10^{10}$ for the lipid membrane (for each of the two flagella). With the total cost of building a *C. reinhardtii* cell being $\simeq 3.2 \times 10^{12}$ ATP hydrolyses (Chapter 8), the relative costs of swimming and constructing the flagellar pair are 0.8 and 2.5%, respectively.

A broader phylogenetic analysis for eukaryotes with small numbers of flagella indicates that, unlike the situation with bacteria, total flagellar construction costs scale hypometrically with cell volume, with a slope $\simeq 0.3$, so that the relative costs decline with increasing cell volume (Figure 16.5b). In contrast, for ciliates and parabasalids (for which the cell is typically coated with small cilia), the scaling relationship is again isometric. Overall, the median total cost of the eukaryotic swimming apparatus relative to the total cell energy budget is $\sim 3\%$, although these costs can be 10 to $100\times$ higher for ciliates and parabasalids than for other eukaryotic flagellates (Figure 16.5c).

Despite the substantial differences in flagellar architecture among prokaryotes and eukaryotes, there is a consistent inverse relationship between the swimming speed (in units of cell length) per construction cost and cell volume across all cellular organisms (Figure 16.5d), with the smallest bacteria having an $\sim 10^4$-fold elevation in this measure of performance relative to the largest ciliates. Thus, as in the case of replication fidelity (Chapter 4) and growth-rate potential (Chapter 8), swimming efficiency is substantially greater in bacteria than in eukaryotes.

Taken together, these results suggest that from an evolutionary perspective, the cost of swimming constitutes a significant fraction of a cell's total energy budget. In accordance with this view, many bacteria have evolved mechanisms for selective use of flagella, restricting their use only to environments providing significant benefits. When confronted with nutrient depletion, some species shed all external features of

their flagella, leaving behind just a plugged remnant of the flagellar motor, whereas others cease assembly, leading to a reduction in flagellum number as the cells divide (Ferreira et al. 2019).

Prolonged periods of silencing of flagellar genes would be expected to eventually lead to the accumulation of deactivating mutations. As such a cascade progresses, there must eventually be a point at which mutation accumulation is so high that reversion to motility is impossible without horizontal gene transfer, and this presumably explains the absence of flagella/cilia from numerous branches in the Tree of Life. However, a remarkable case of the resurrection of a flagellum was observed in an experimental construct of the bacterium *Pseudomonas fluorescens* engineered to be nonmotile by deletion of a key regulatory gene for flagellar gene expression (Taylor et al. 2015). After just four days of strong selection for motility, this bacterium regained flagella as mutations redirected a regulatory gene for nitrogen assimilation towards the promotion of expression of still intact flagellar genes (albeit at the expense of nitrogen uptake).

Finally, there is the issue of why prokaryotes and eukaryotes evolved such dramatically different flagellum types. As noted by Schavemaker and Lynch (2022), the cost of eukaryotic flagella per flagellum unit length substantially exceeds that for prokaryotes. Were bacteria to expend their normal flagellar construction costs on a flagellum of the eukaryotic form, the latter would be extremely short and unlikely to elicit much motility. This raises the possibility that the eukaryotic flagellum arose in a pre-LECA ancestor devoid of a bacterial-like flagellum, absolving it from competing with such a form, while also requiring an expansion in cell size to a level that could support the magnified construction costs.

Summary

- Eukaryotic cells rely heavily on polymers of monomeric (actin) or heterodimeric (tubulin) protein subunits concatenated into linear fibrils. Such constructs are used in a variety of cellular functions, ranging from structural support to intracellular vesicle trafficking to motility.

- Although less apparent visually, evolutionary relatives of such filaments are also found in prokaryotes. This implies their presence at the time of the last universal common ancestor, with subsequent functional modifications arising in the eukaryotic domain. Shifts in the deployment of tubulins vs. actins for different functions between the major domains of life provide dramatic examples of convergent/divergent evolution of cellular functions at the molecular level.

- Scaled to the total costs of constructing cells, the investment in fibrillar proteins in eukaryotes ($\simeq 0.5$ to 4%) may be only two-fold greater than it is in prokaryotes.

- Cell sizes and shapes are sustained by endoskeletons (fibrillar proteins) and/or

exoskeletons (cell walls). Although the detailed genetic mechanisms underlying cell-shape homeostasis and the evolutionary mechanisms driving shape changes are largely unknown in eukaryotes, substantial shifts in the geometric features of bacterial cells can be accomplished by just single amino-acid changes in one or two proteins.

- Many species deploy hard cell coverings, either internal or external to the plasma membrane. These provide resistance to turgor pressure and likely have other functions such as avoiding predation. Although peptidoglycans (prokaryotes) and cellulose and chitin (eukaryotes) are common components of cell walls, numerous variants are deployed across eukaryotic phylogeny, including the use of inorganic components (e.g., silicon and calcium) in some lineages.

- The investment in cell walls can be quite substantial, accounting for as much as half the costs of the complete cell envelope, with the latter (including lipid membranes) comprising on the order of 20 to 40% of a cell's lifetime energy budget. These numbers are strikingly similar to the realtor's rule-of-thumb that one should spend no more than one-third of one's income on a home.

- Whereas most intracellular transport in bacteria is accomplished by passive diffusion, eukaryotic cells deploy molecular motors to carry large cargoes, such as vesicles, using the cytoskeleton as a structural highway. Three major classes of molecular motors exist within eukaryotes (kinesins, myosins, and dyneins), all of which diversified into multiple subfamilies with different subfunctions prior to the last eukaryotic common ancestor.

- The most complex morphological structure of most prokaryotic cells is the flagellum, whose origin seems rooted to structures used in ATP synthase and in secretion systems, with the overall elaborations having arisen in part by gene duplication. Numerous eukaryotes also swim with flagella, but the eukaryotic flagellum evolved independently of that in prokaryotes and operates in a fundamentally different way, using cytoskeletal and motor proteins.

- In units of body lengths, swimming rates are several times higher in prokaryotes than eukaryotes, but their operating costs per unit volume are also higher. The efficiency of conversion of chemical to mechanical energy used in motion is quite low (of order 1%). As a fraction of a cell's total energy budget, the costs of flagella are on the order of 0.1 to 1.0%, with the costs of construction and operation being of similar magnitudes. Thus, there is a strong selective premium for eliminating flagella unless the advantages outweigh the costs.

Foundations 16.1. The eukaryotic cellular investment in the cytoskeleton. Given the central roles that the cytoskeletal proteins (actin and tubulin) play in eukaryotic cell biology, it is of interest to evaluate the fraction of the cell's energy budget devoted to their production. Estimates are available for the average number of monomers of each protein within the cells of a few species, and this information combined with the cost of protein biosynthesis (to be covered in more detail in Chapter 17) and the cost of building an entire cell (Chapter 8) can be used to obtain a rough estimate of the relative cost of the cytoskeleton.

For the two model yeast species, the average numbers of actin and tubulin monomers per cell are, respectively: 88,600 and 22,400 for *S. cerevisiae* (Norbeck and Blomberg 1997; Kulak et al. 2014); and 731,500 and 125,100 for *S. pombe* (Wu and Pollard 2005; Marguerat et al. 2012; Kulak et al. 2014). Together, these two molecules account for $\sim 0.24\%$ and 0.77% of the total number of proteins per cell in *S. cerevisiae* and *S. pombe,* respectively.

These numbers can be converted into bioenergetic-cost estimates by noting that: 1) actin and tubulin monomers contain ~ 375 and 450 amino acids, respectively; and 2) the average cost of amino-acid biosynthesis is 30 ATP hydrolyses per amino acid, with another 4 hydrolyses necessary for polypeptide-chain elongation (Chapter 17). Taking the total cost (in ATP hydrolyses per cell cycle) to be the product of the number of monomers, the number of amino acids per monomer, and 34 ATP hydrolyses per amino-acid residue leads to estimates of 1.1×10^9 and 3.3×10^8 for actin and tubulin in *S. cerevisiae,* and 9.1×10^9 and 1.9×10^9 in *S. pombe.* There are additional costs associated with transcription of the genes for these proteins, but as will be more fully discussed in Chapter 17, about 90% of the total cost of running genes is associated with protein production, so the above numbers are only slight underestimates.

To put this into broader perspective, recall that Equation 8.2b provides an estimate of the cost of building an entire cell. Given cell volumes of $\sim 70\,\mu\text{m}^3$ for *S. cerevisiae* and $130\,\mu\text{m}^3$ for *S. pombe,* the number of ATP hydrolyses required for the construction of cells in these two species $\simeq 1.5\times10^{12}$ and 2.9×10^{12}, respectively. Thus, just 0.1 and 0.4% of the total energy budgets for cell construction in these species is devoted to the cytoskeleton, with $\sim 80\%$ of such costs being associated with actin. Similar calculations using data from mouse fibroblast cells (Schwanhäusser et al. 2011) lead to estimates of 3.8% for actins and 1.9% for tubulins, and for human HeLa cells (Kulak et al. 2014) of 0.1% for actins and 0.5% for tubulins.

What can be said of such investments in prokaryotes? Although few quantitative data are available, the two major cytoskeletal proteins in *E. coli,* FtsZ (related to actin) and MreB (related to tubulin), have average abundances of 3,450 and 1,060 protein monomers per cell (Pla et al. 1991; Rueda et al. 2003; Lu et al. 2007; Taniguchi et al. 2010; Wiśniewski and Rakus 2014; Vischer et al. 2015; Ousounov et al. 2016; Bratton et al. 2018), with respective contents of 383 and 347 amino acids/monomer. With the cost of building an *E. coli* cell being $\simeq 27 \times 10^9$ ATP hydrolyses (Chapter 8), the fractional contributions of these two molecules to the total cell budget are 0.16 and 0.04%, respectively. Thus, although the common view is that eukaryotes invest substantially more in cytoskeletal infrastructure than do prokaryotes, this simple comparison suggests a comparable cost in yeasts and *E. coli,* with an inflation in metazoan cells.

Foundations 16.2. The physical challenges to cellular locomotion. A key to understanding the relative advantages / disadvantages of motility in single-celled

organisms is in quantifying the way in which the resistance of a fluid to the motion of an object scales with the size of the object (Purcell 1977). The central concept is related to the definition of a dimensionless index known as the Reynolds number, which equals the ratio of inertial to viscous forces,

$$\mathrm{Re} = \frac{\rho v L}{\eta}, \tag{16.2.1}$$

where ρ is the fluid density (g/cm^3), v is the velocity of the object (cm/sec), L is the characteristic linear dimension of the object (which depends on the shape; cm), and η is the fluid viscosity (g/cm·sec). For water, $\eta/\rho \simeq 10^{-2}$ cm^2/sec. Although the source of Equation 16.2.1 may not be intuitive, the derivation follows from the fact that the inertial force of an object (the numerator in Re) is equal to mass times acceleration (the rate of change of velocity), i.e., $(\rho L^3) \cdot (v/t)$, where t denotes time. The denominator follows from the definition of the coefficient of viscosity (η) as the viscous force per unit area per the velocity gradient (change in velocity per distance), which gives a total viscosity force of $\eta \cdot L^2 \cdot (v/L)$. Noting that $(v/t)/(v/L) = L/t$ is equivalent to v reduces to $[\,(\rho L^3) \cdot (v/t)\,]/[\,\eta \cdot L^2 \cdot (v/L)\,]$ to Equation 16.2.1.

The Reynolds number is a convenient index of the challenges confronted by an object moving in a fluid. When $\mathrm{Re} < 1$, viscous forces dominate, and in the limiting case of $\mathrm{Re} \ll 1$, the motion at any particular moment is essentially independent of all prior action. In the latter case, the resistance of the fluid is so great that movement of the object ceases nearly instantaneously if the force of motion is stopped. Almost all aspects of cellular movement are in this low Reynolds number range. For example, as noted above for bacterial motility, v is almost always $< 100\,\mu$m/sec, and most bacterial cells have lengths of order $1\,\mu$m, so given that $1\,\mu\mathrm{m} = 10^{-4}$ cm, Re is on the order of 10^{-4}.

A key definition from physics is that power (the rate of doing work, or equivalently the rate of energy utilization) is equal to the product of force and velocity, $P = F \cdot v$. From Stokes' law, which specifically applies to low Reynolds number situations, the inertial drag force for a sphere with radius r is $F = 6\pi r\eta v$, so

$$P = 6\pi r\eta v^2. \tag{16.2.2}$$

The formula differs for different shapes (see pages 56-57, Berg (1993) for some approximations, and Perrin (1934, 1936) for more general results), although the scaling with ηv^2 remains. One has to be careful with units here. If F has units of kg-m/sec^2, and v has units of m/sec, then P has units of watts or joules/sec. To determine the total metabolic power required to maintain velocity v, the preceding expression must be divided by the efficiency of conversion of electrochemical energy to directional motion (i.e., the ratio of propulsive-power output to rotary-power input), which in *E. coli* is estimated to be 0.017 (Chattopadhyay et al. 2006; see main text for other estimates).

To determine the potential benefits of swimming in terms of resource acquisition, consider the overall process as being equivalent to a measure of effective diffusion of the cell through the medium. Suppose a cell swims for time τ with constant velocity v in a three-dimensional environment, pauses for infinitesimally short time, and then randomly starts off in a new direction, with the swimming durations being exponentially distributed. Although the physical length of each individual bout is $v\tau$, the runs are distributed over three dimensions (Chapter 7). Because the times are exponentially distributed, with variance $(\overline{\tau^2} - \overline{\tau}^2)$ equal to the square of the mean, the average squared value of run times is $\overline{\tau^2} = 2\overline{\tau}^2$. Thus, the mean-squared length of movement per bout is $2v^2\overline{\tau}^2/3$. By definition, the mean-squared deviation of movement in τ time units is $2D\tau$ (Chapter 7), where D is the diffusion coefficient. Equating these two expressions and factoring out 2τ leads to

$$D = \frac{v^2\tau}{3} \tag{16.2.3a}$$

under the assumption that the directions of movement between adjacent steps are random.

If there is some memory of the swimming process such that successive bouts tend to go roughly in the same direction, the average distance traveled is expected to increase. If, however, there is a tendency to switch to opposing directions, the cumulative distance traveled will be decreased. Such correlations of movement can be accommodated by dividing the previous expression by $(1 - \overline{c})$, where $\overline{c}$ is the mean cosine of the angle of switching (Lovely and Dahlquist 1975),

$$D = \frac{v^2\overline{\tau}}{3(1-\overline{c})}. \tag{16.2.3b}$$

If the angle of switching is small, $(1 - \overline{c}) \simeq \overline{\theta^2}/2$, where θ is in radians. The mean-squared angular (rotational) deviation $\overline{\theta^2}/2$ is analogous to the mean-squared linear (translational) movement encountered in Chapter 7, leading to the concept of rotational diffusion. By definition, $\overline{\theta^2}/2 = 2D_r\overline{\tau}$, where D_r is the rotational diffusion coefficient.

Even in the absence of behaviorally-induced switching of angles, the jostling of fluid molecules causes rotational diffusion of the cell, just as in the case of translational diffusion. It is known that under these conditions $D_r = k_BT/(8\pi\eta r^3)$ (Berg 1993; Equation 6.6). This inverse relationship between the rate of rotational diffusion and cell size means that directional swimming becomes increasingly challenging in small cells that are continually being reoriented by physical forces (Mitchell 1991). Using the preceding approximation for $(1 - \overline{c})$, this leads to an effective diffusion rate of

$$D = \frac{v^2\overline{\tau}}{3(1-\overline{c})} = \frac{2v^2\overline{\tau}}{3\overline{\theta^2}} = \frac{v^2}{6D_r} = \frac{4\pi\eta r^3 v^2}{3k_BT}. \tag{16.2.4a}$$

for a cell at the mercy of random thermal jostling. From Chapter 2, we know that $k_BT \simeq 4.1 \times 10^{-14}$ cm$^2 \cdot$ g $\cdot$ sec^{-2}, and for water $\eta \simeq 10^{-3}$ g $\cdot$ cm$^{-1} \cdot$ sec^{-1}, so for a cell in a freshwater environment, subject to translational and rotational diffusion

$$D \simeq 10^{12} \cdot r^3 v^2, \tag{16.2.4b}$$

where r and v have units of cm and cm/sec, respectively, yielding D with units of cm^2/sec.

The preceding expressions can be used to estimate the influence of swimming on the encounter rate of molecules. For example, if one considers a bacterium with typical $r \simeq 10^{-4}$ cm, and $v \simeq 3 \times 10^{-3}$ cm/sec, then assuming randomly directed swimming, the effective diffusion coefficient for the cell is $D \simeq 10^{-5}$ cm^2/sec. From Figure 7.6, the average diffusion coefficient for a typical anion/cation is also $\simeq 10^{-5}$ cm^2/sec, with that for a protein containing 100 amino acids being $\simeq 10^{-6}$ cm^2/sec. The encounter rate between two different types of diffusing particles is proportional to the sum of their diffusion coefficients. Thus, without direct behavioral modifications of swimming direction, a swimming bacterial cell can encounter randomly distributed resources at a rate at least double that expected for a nonmotile cell, and larger, more rapidly swimming cells will achieve more. There are, however, some subtle complications not dealt with here, most notably the fact that a boundary layer of nutrient-depleted fluid adheres to swimming cells, thereby reducing the effective concentration of resources to a degree that declines with swimming speed (Chapter 18).

Behavioral mechanisms can substantially magnify average levels of resource availability by biasing movement towards resource-rich patches in a heterogeneous environment. For example, an ability to respond to local resource abundance (e.g., by chemotaxis; Chapter 22) can enhance encounter rates by fostering a positive directional bias

of movement up a resource gradient. Likewise, a negative bias can lead to local retention in a nutrient-rich patch. Consider, for example, a strong positive correlation of directional movement, $\overline{c} = 0.9$. Applying this to the left-most expression in Equation 16.2.4a, with a bacterial swimming speed of $v \simeq 3 \times 10^{-3}$ cm/sec and $\overline{\tau} = 1$ sec, leads to $D \simeq 3 \times 10^{-5}$ cm^2/sec, whereas $\overline{c} = 0$ (random movement) leads to $D \simeq 3 \times 10^{-6}$, and $\overline{c} = -0.8$ leads to $D \simeq 1.7 \times 10^{-6}$ cm^2/sec.

Arguments like these provide a starting point for estimating costs and benefits of locomotion and chemoreception. Based on a metabolic scaling argument, Dusenbery (1997) estimates that there is a minimal size limit of ~ 0.8 μm below which there is no advantage to motility, although his arguments ignore the cost of building the motility apparatus (Foundations 16.3). If one computes the Sherwood number (a measure of the encounter rate of nutrients in a swimming cell relative to that expected by passive diffusion in a nonmotile cell; Foundations 18.1) and compares that to the ratio of construction costs of swimming and nonmotile cells, it is found that the flagella for bacterial-sized cells cannot be paying for themselves in terms of increased nutrient accessibility (Schavemaker and Lynch 2022). Whereas swimming does have such an advantage in moderate- to large-sized eukaryotic cells, motility in bacteria must be associated with other advantages such as location of nutrient-rich patches.

Foundations 16.3. The construction costs of flagella. The cost of building a molecular machine such as a flagellum can be estimated using the general methodology outlined in Foundations 16.1 (with further elaborations on the underpinnings in Chapter 17). For a bacterial flagellum, the biosynthetic costs can be roughly computed as follows. From Berg (2003), an average *E. coli* flagellar filament contains ~ 5340 flagellin protein molecules, each containing ~ 500 amino acids, implying a total investment of $\sim 2.7 \times 10^6$ amino acids/flagellar filament. The remaining proteins associated with the basal body, rod, and hook comprise only about 5% of the protein in the flagellum (Sosinsky et al. 1992; Berg 2003), so in total there are $\sim 3 \times 10^6$ amino acids involved. As noted in Foundations 17.2, the total translation-associated cost per amino acid (including synthesis and polymerization) is ~ 34 ATP hydrolyses, and additional costs of genes at the DNA and mRNA levels only inflate these estimates by $\sim 10\%$. This implies a protein biosynthetic cost per *E. coli* flagellum of $\sim 10^8$ ATP hydrolyses. Supplementing this estimate with the costs of the flagellar export-apparatus proteins, Schavemaker and Lynch (2022) obtained an estimate of 2×10^8.

For some bacteria, there is an additional cost of wrapping the filament with a lipid membrane. Although not one of these, *E. coli* will nonetheless be used here to examine the consequences of such an elaboration. Again, the details underlying the computations will be given in Chapter 17. The essential points are that with an average *E. coli* flagellum radius and length of 0.01 and 6 μm, respectively, the cylindrical surface area of the flagellum is $\sim 0.4\,\mu$m^2. As the average membrane area occupied by a bacterial lipid molecule is $0.65 \times 10^{-6}\,\mu$m^2, after accounting for the two leaflets of the lipid bilayer, there would be an estimated 1.2×10^6 lipid molecules surrounding this flagellum. The biosynthetic costs of lipids are much greater than those for proteins, averaging 300 ATP hydrolyses per lipid molecule, leading to a total biosynthetic cost of the hypothetical flagellar membrane of $\sim 3.6 \times 10^8$ ATP hydrolyses, $\sim 2\times$ that of the protein components.

To extend these calculations to eukaryotes, consider the green alga *Chlamydomonas reinhardtii,* which generally has two flagella with approximate radii and lengths of 0.075 and 20 μm. After accounting for the slightly elevated cost of lipid biosynthesis in eukaryotes ($\simeq 350$ ATPs), this implies a total membrane cost surrounding each flagellum of $\sim 10^{10}$ ATP. Raven and Richardson (1984) estimate there to be $\sim 48,000$ tubulin monomers (each ~ 450 amino acids in length) per μm of flagellum,

implying a cost for this major molecule of $\sim 1.5 \times 10^{10}$ ATP. There are also ~ 600 copies of the large motor protein dynein (each $\sim 15,000$ amino acids in length) per μm, implying an additional construction cost of $\sim 6.1 \times 10^9$ ATP. There are numerous other proteins within eukaryotic flagella, including the smaller motor protein kinesin, but their summed number is unlikely to rival that for tubulin and dynein, so the total cost of protein synthesis associated with each *C. reinhardtii* flagellum is $\sim 3 \times 10^{10}$ ATP. This is $\sim 3\times$ the lipid cost, opposite the situation for a bacterial flagellum, but expectedly so, given the lower surface area:volume ratio of the thicker eukaryotic flagellum. A much more detailed accounting in Schavemaker and Lynch (2022) yields similar estimates.

For further information on these matters, including the costs of archaeal flagella, see Schavemaker and Lynch (2022).

Literature Cited

Akhmanova, A., and M. O. Steinmetz. 2015. Control of microtubule organization and dynamics: two ends in the limelight. Nat. Rev. Mol. Cell. Biol. 16: 711-726.

Albers, S. V., and K. F. Jarrell. 2018. The archaellum: an update on the unique archaeal motility structure. Trends Microbiol. 26: 351-362.

Albers, S. V., and B. H. Meyer. 2011. The archaeal cell envelope. Nat. Rev. Microbiol. 9: 414-426.

Albers, S. V., and M. Pohlschröder. 2009. Diversity of archaeal type IV pilin-like structures. Extremophiles 13: 403-410.

Alliegro, M. C., and P. Satir. 2009. Origin of the cilium: novel approaches to examine a centriolar evolution hypothesis. Methods Cell Biol. 94: 53-64.

Amir, A., F. Babaeipour, D. B. McIntosh, D. R. Nelson, and S. Jun. 2014. Bending forces plastically deform growing bacterial cell walls. Proc. Natl. Acad. Sci. USA 111: 5778-5783.

Arroyo, M., L. Heltai, D. Millán, and A. DeSimone. 2012. Reverse engineering the euglenoid movement. Proc. Natl. Acad. Sci. USA 109: 17874-17879.

Asmar, A. T., and J. F. Collet. 2018. Lpp, the Braun lipoprotein, turns 50-major achievements and remaining issues. FEMS Microbiol. Lett. 365 (18).

Avidor-Reiss, T., A. M. Maer, E. Koundakjian, A. Polyanovsky, T. Keil, S. Subramaniam, and C. S. Zuker. 2004. Decoding cilia function: defining specialized genes required for compartmentalized cilia biogenesis. Cell 117: 527-539.

Barsanti, L., P. Coltelli, V. Evangelista, A. M. Frassanito, and P. Gualtieri. 2016. Swimming patterns of the quadriflagellate *Tetraflagellochloris mauritanica* (Chlamydomonadales, Chlorophyceae). J. Phycol. 52: 209-218.

Bazylinski, D. A., and R. B. Frankel. 2004. Magnetosome formation in prokaryotes. Nat. Rev. Microbiol. 2: 217-230.

Becker, B. 2000. The cell surface of flagellates, pages 110-123. In B. S. C. Leadbeater and J. C. G. Taylor (eds.) The Flagellates: Unity, Diversity, and Evolution. Taylor and Francis, New York, NY.

Berg, H. C. 1993. Random Walks in Biology. Princeton Univ. Press, Princeton, NJ.

Berg, H. C. 2003. The rotary motor of bacterial flagella. Annu. Rev. Biochem. 72: 19-54.

Bernander, R., and T. J. Ettema. 2010. FtsZ-less cell division in archaea and bacteria. Curr. Opin. Microbiol. 13: 747-752.

Billaudeau, C., A. Chastanet, Z. Yao, C. Cornilleau, N. Mirouze, V. Fromion, and R. Carballido-López. 2017. Contrasting mechanisms of growth in two model rod-shaped bacteria. Nat. Commun. 8: 15370.

Block, S. M., L. S. Goldstein, and B. J. Schnapp. 1990. Bead movement by single kinesin molecules studied with optical tweezers. Nature 348: 348-352.

Blocker, A., K. Komoriya, and S. Aizawa. 2003. Type III secretion systems and bacterial flagella: insights into their function from structural similarities. Proc. Natl. Acad. Sci. USA 100: 3027-3030.

Boehm, A., M. Kaiser, H. Li, C. Spangler, C. A. Kasper, M. Ackermann, V. Kaever, V. Sourjik, V. Roth, and U. Jenal. 2010. Second messenger-mediated adjustment of bacterial swimming velocity. Cell 141: 107-116.

Bork, P., C. Sander, and A. Valencia. 1992. An ATPase domain common to prokaryotic cell cycle proteins, sugar kinases, actin, and hsp70 heat shock proteins. Proc. Natl. Acad. Sci. USA 89: 7290-7294.

Bratton, B. P., J. W. Shaevitz, Z. Gitai, and R. M. Morgenstein. 2018. MreB polymers and curvature localization are enhanced by RodZ and predict *E. coli*'s cylindrical uniformity. Nat. Commun. 9: 2797.

Braun, T., A. Orlova, K. Valegård, A. C. Lindås, G. F. Schröder, and E. H. Egelman. 2015. Archaeal actin from a hyperthermophile forms a single-stranded filament. Proc. Natl. Acad. Sci. USA 112: 9340-9345.

Brunet, T., M. Albert, W. Roman, M. C. Coyle MC, D. C. Spitzer, and N. King. 2021. A flagellate-to-amoeboid switch in the closest living relatives of animals. eLife 10: e61037.

Carlier, M. F., and S. Shekhar. 2017. Global treadmilling coordinates actin turnover and controls the size of actin networks. Nat. Rev. Mol. Cell. Biol. 18: 389-401.

Carvalho-Santos, Z., J. Azimzadeh, J. B. Pereira-Leal, and M. Bettencourt-Dias. 2011. Evolution: tracing the origins of centrioles, cilia, and flagella. J. Cell Biol. 194: 165-175.

Carvalho-Santos, Z., P. Machado, P. Branco, F. Tavares-Cadete, A. Rodrigues-Martins, J. B. Pereira-Leal, and M. Bettencourt-Dias. 2010. Stepwise evolution of the centriole-assembly pathway. J. Cell Sci. 123: 1414-1426.

Cavalier-Smith, T. 1978. The evolutionary origin and phylogeny of microtubules, mitotic spindles and eukaryote flagella. Biosystems 10: 93-114.

Cavalier-Smith, T. 2002. The phagotrophic origin of eukaryotes and phylogenetic classification of Protozoa. Internat. J. Syst. Evol. Microbiol. 52: 297-354.

Chaban, B., I. Coleman, and M. Beeby. 2018. Evolution of higher torque in *Campylobacter*-type bacterial flagellar motors. Sci. Rep. 8: 97.

Chattopadhyay, S., R. Moldovan, C. Yeung, and X. L. Wu. 2006. Swimming efficiency of bacterium *Escherichia coli*. Proc. Natl. Acad. Sci. USA 103: 13712-13717.

Chen, S., M. Beeby, G. E. Murphy, J. R. Leadbetter, D. R. Hendrixson, A. Briegel, Z. Li, J. Shi, E. I. Tocheva, A. Müller, et al. 2011. Structural diversity of bacterial flagellar motors. EMBO J. 30: 2972-2981.

Chia, F.-S., J. Buckland-Nicks, and C. M. Young. 1984. Locomotion of marine invertebrate larvae: a review. Can. J. Zool. 62: 1205-1222.

Cochran, J. C. 2015. Kinesin motor enzymology: chemistry, structure, and physics of nanoscale molecular machines. Biophys. Rev. 7: 269-299.

Crawford, D. W. 1992. Metabolic cost of motility in planktonic protists: theoretical considerations on size scaling and swimming speed. Microb. Ecol. 24: 1-10.

Daum, B., J. Vonck, A. Bellack, P. Chaudhury, R. Reichelt, S. V. Albers, R. Rachel, and W. Kühlbrandt. 2017. Structure and *in situ* organisation of the *Pyrococcus furiosus* archaellum machinery. eLife 6: e27470.

Deng, X., G. Fink, T. A. M. Bharat, S. He, D. Kureisaite-Ciziene, and J. Löwe. 2017. Four-stranded mini microtubules formed by *Prosthecobacter* BtubAB show dynamic instability. Proc. Natl. Acad. Sci. USA 114: E5950-E5958.

Desmond, E., C. Brochier-Armanet, and S. Gribaldo. 2007. Phylogenomics of the archaeal flagellum: rare horizontal gene transfer in a unique motility structure. BMC Evol. Biol. 7: 106.

Dion, M. F., M. Kapoor, Y. Sun, S. Wilson, J. Ryan, A. Vigouroux, S. van Teeffelen, R. Oldenbourg, and E. C. Garner. 2019. *Bacillus subtilis* cell diameter is determined by the opposing actions of two distinct cell wall synthetic systems. Nat. Microbiol. 4: 1294-1305.

Dishinger, J. F., H. L. Kee, P. M. Jenkins, S. Fan, T. W. Hurd, J. W. Hammond, Y. N. Truong, B. Margolis, J. R. Martens, and K. J. Verhey. 2010. Ciliary entry of the kinesin-2 motor KIF17 is regulated by importin-beta2 and RanGTP. Nat. Cell Biol. 12: 703-710.

Domozych, D. S., I. Sørensen, Z. A. Popper, J. Ochs, A. Andreas, J. U. Fangel, A. Pielach, C. Sacks, H. Brechka, P. Ruisi-Besares, et al. 2014. Pectin metabolism and assembly in the cell wall of the charophyte green alga *Penium margaritaceum.* Plant Physiol. 165: 105-118.

Dusenbery, D. B. 1997. Minimum size limit for useful locomotion by free-swimming microbes. Proc. Natl. Acad. Sci. USA 94: 10949-10954.

Dusenbery, D. B. 1998. Fitness landscapes for effects of shape on chemotaxis and other behaviors of bacteria. J. Bacteriol. 180: 5978-5983.

Dutcher, S. K. 2003. Long-lost relatives reappear: identification of new members of the tubulin superfamily. Curr. Opin. Microbiol. 6: 634-640.

Egelman, E. H. 2010. Reducing irreducible complexity: divergence of quaternary structure and function in macromolecular assemblies. Curr. Opin. Cell Biol. 22: 68-74.

Elting, M. W., Z. Bryant, J. C. Liao, and J. A. Spudich. 2011. Detailed tuning of structure and intramolecular communication are dispensable for processive motion of myosin VI. Biophys. J. 100: 430-439.

Erickson, H. P. 2007. Evolution of the cytoskeleton. Bioessays 29: 668-677.

Ettema, T. J., A. C. Lindås, and R. Bernander. 2011. An actin-based cytoskeleton in archaea. Mol. Microbiol. 80: 1052-1061.

Fai, T. G., L. Mohapatra, P. Kar, J. Kondev, and A. Amir. 2019. Length regulation of multiple flagella that self-assemble from a shared pool of components. eLife 8: e42599.

Fenchel, T., and B. J. Finlay. 1983. Respiration rates in heterotrophic, free-living protozoa. Microb. Ecol. 9: 99-122.

Ferreira, J. L., F. Z. Gao, F. M. Rossmann, A. Nans, S. Brenzinger, R. Hosseini, A. Wilson, A. Briegel, K. M. Thormann, P. B. Rosenthal, et al. 2019. γ-proteobacteria eject their polar flagella under nutrient depletion, retaining flagellar motor relic structures. PLoS Biol. 17: e3000165.

Flamholz, A., R. Phillips, and R. Milo. 2014. The quantified cell. Mol. Biol. Cell 25: 3497-3500.

Foth, B. J., M. C. Goedecke, and D. Soldati. 2006. New insights into myosin evolution and classification. Proc. Natl. Acad. Sci. USA 103: 3681-3686.

Fritz-Laylin, L. K., S. J. Lord, and R. D. Mullins. 2017. WASP and SCAR are evolutionarily conserved in actin-filled pseudopod-based motility. J. Cell Biol. 216: 1673-1688.

Fulton, C. 1977. Cell differentiation in *Naegleria gruberi.* Annu. Rev. Microbiol. 31: 597-629.

Galkin, V. E., X. Yu, J. Bielnicki, J. Heuser, C. P. Ewing, P. Guerry, and E. H. Egelman. 2008. Divergence of quaternary structures among bacterial flagellar filaments. Science 320: 382-385.

Gardner, M. K., M. Zanic, and J. Howard. 2013. Microtubule catastrophe and rescue. Curr. Opin. Cell. Biol. 25: 14-22.

Geis, G, Suerbaum S, Forsthoff B, Leying H, and Opferkuch W. 1993. Ultrastructure and biochemical studies of the flagellar sheath of *Helicobacter pylori.* J. Med. Microbiol. 38: 371-377.

Ghoshdastider, U., S. Jiang, D. Popp, and R. C. Robinson. 2015. In search of the primordial actin filament. Proc. Natl. Acad. Sci. USA 112: 9150-9151.

Gilbert, J. J. 1994. Jumping behavior in the oligotrich ciliates *Strobilidium velox* and *Halteria grandinella,* and its significance as a defense against rotifer predators. Microb. Ecol. 27: 189-200.

Ginger, M. L., N. Portman, and P. G. McKean. 2008. Swimming with protists: perception, motility and flagellum assembly. Nat. Rev. Microbiol. 6: 838-850.

Gittleson, S. M., and R. M. Noble. 1973. Locomotion in *Polytomella agilis* and *Polytoma uvella.* Trans. Amer. Micro. Soc. 92: 122-128

Gönczy, P. 2012. Towards a molecular architecture of centriole assembly. Nat. Rev. Mol. Cell Biol. 13: 425-435.

Goodson, H. V., and S. C. Dawson. 2006. Multiplying myosins. Proc. Natl. Acad. Sci. USA 103: 3498-3499.

Goodson, H. V., and W. F. Hawse. 2002. Molecular evolution of the actin family. J. Cell Sci. 115: 2619-2622.

Gumbart, J. C., M. Beeby, G. J. Jensen, and B. Roux. 2014. *Escherichia coli* peptidoglycan structure and mechanics as predicted by atomic-scale simulations. PLoS Comput. Biol. 10: e1003475.

Hariharan, V., and W. O. Hancock. 2009. Insights into the mechanical properties of the kinesin neck linker domain from sequence analysis and molecular dynamics simulations. Cell. Mol. Bioeng. 2: 177-189.

Hartman, H., and T. F. Smith. 2009. The evolution of the cilium and the eukaryotic cell. Cell Motil. Cytoskeleton 66: 215-219.

Hartmann, E., and H. König. 1990. Comparison of the biosynthesis of the methanobacterial pseudomurein and the eubacterial murein. Naturwissenschaften 77: 472-475.

Hodges, M. E., N. Scheumann, B. Wickstead, J. A. Langdale, and K. Gull. 2010. Reconstructing the evolutionary history of the centriole from protein components. J. Cell Sci. 123: 1407-1413.

Horio, T., and B. R. Oakley. 1994. Human gamma-tubulin functions in fission yeast. J. Cell. Biol. 126: 1465-1473.

Hou, Y., R. Sierra, D. Bassen, N. K. Banavali, A. Habura, J. Pawlowski, and S. S. Bowser. 2013. Molecular evidence for β-tubulin neofunctionalization in Retaria (Foraminifera and radiolarians). Mol. Biol. Evol. 30: 2487-2493.

Howard, J. 2001. Mechanics of Motor Proteins and the Cytoskeleton. Sinauer Assocs., Inc. Sunderland, MA.

Hwang, W., and Karplus M. 2019. Structural basis for power stroke vs. Brownian ratchet mechanisms of motor proteins. Proc. Natl. Acad. Sci. USA 116: 19777-19785.

Ishikawa, H., and W. F. Marshall. 2011. Ciliogenesis: building the cell's antenna. Nat. Rev. Mol. Cell Biol. 12: 222-234.

Ishikawa, H., and W. F. Marshall. 2017. Testing the time-of-flight model for flagellar length sensing. Mol. Biol. Cell. 28: 3447-3456.

Ito, M., and Y. Takahashi. 2017. Nonconventional cation-coupled flagellar motors derived from the alkaliphilic *Bacillus* and *Paenibacillus* species. Extremophiles 21: 3-14.

Izoré, T., D. Kureisaite-Ciziene, S. H. McLaughlin, and J. Löwe. 2016. Crenactin forms actin-like double helical filaments regulated by arcadin-2. eLife 5: e21600.

Jarrell, K. F., and M. J. McBride. 2008. The surprisingly diverse ways that prokaryotes move. Nat. Rev. Microbiol. 6: 466-476.

Jékely, G., and D. Arendt. 2006. Evolution of intraflagellar transport from coated vesicles and autogenous origin of the eukaryotic cilium. Bioessays 28: 191-198.

Joseph, J. M., P. Fey, N. Ramalingam, X. I. Liu, M. Rohlfs, A. A. Noegel, A. Müller-Taubenberger, G. Glöckner, and M. Schleicher. 2008. The actinome of *Dictyostelium discoideum* in comparison to actins and actin-related proteins from other organisms. PLoS One 3: e2654.

Kaplan, M., D. Ghosal, P. Subramanian, C. M. Oikonomou, A. Kjaer, S. Pirbadian, D. R. Ortega, A. Briegel, M. Y. El-Naggar, and G. J. Jensen. 2019. The presence and absence of periplasmic rings in bacterial flagellar motors correlates with stator type. eLife 8: e43487.

Kardon, J. R., and R. D. Vale. 2009. Regulators of the cytoplasmic dynein motor. Nat. Rev. Mol. Cell. Biol. 10: 854-865.

Katsu-Kimura, Y., F. Nakaya, S. A. Baba, and Y. Mogami. 2009. Substantial energy expenditure for locomotion in ciliates verified by means of simultaneous measurement of oxygen consumption rate and swimming speed. J. Exp. Biol. 212: 1819-1824.

Kee, H. L., J. F. Dishinger, T. L. Blasius, C. J. Liu, B. Margolis, and K. J. Verhey. 2012. A size-exclusion permeability barrier and nucleoporins characterize a ciliary pore complex that regulates transport into cilia. Nat. Cell Biol. 14: 431-437.

Khona, D. K., V. G. Rao, M. J. Motiwalla, P. C. Sreekrishna Varma, A. R. Kashyap, K. Das, S. M. Shirolikar, L. Borde, J. A. Dharmadhikari, A. K. Dharmadhikari, et al. 2013. Anomalies in the motion dynamics of long-flagella mutants of *Chlamydomonas reinhardtii.* J. Biol. Phys. 39: 1-14.

Kiefel, B. R., P. R. Gilson, and P. L. Beech. 2004. Diverse eukaryotes have retained mitochondrial homologues of the bacterial division protein FtsZ. Protist 155: 105-115.

Kinosita, Y., N. Uchida, D. Nakane, and T. Nishizaka. 2016. Direct observation of rotation and steps of the archaellum in the swimming halophilic archaeon *Halobacterium salinarum.* Nat. Microbiol. 1: 16148.

Klis, F. M., C. G. de Koster, and S. Brul. 2014. Cell wall-related bionumbers and bioestimates of *Saccharomyces cerevisiae* and *Candida albicans.* Eukaryot. Cell 13: 2-9.

Kollmar, M., D. Lbik, and S. Enge. 2012. Evolution of the eukaryotic ARP2/3 activators of the WASP family WASP, WAVE, WASH, and WHAMM, and the proposed new family members WAWH and WAML. BMC Res. Notes 5: 88.

Kreutzberger, M. A. B., R. R. Sonani, J. Liu, S. Chatterjee, F. Wang, A. L. Sebastian, P. Biswas, C. Ewing, W. Zheng, F. Poly, et al. 2022. Convergent evolution in the supercoiling of prokaryotic flagellar filaments. Cell 185: 3487-3500.e14.

Kulak, N. A., G. Pichler, I. Paron, N. Nagaraj, and M. Mann. 2014. Minimal, encapsulated proteomic-sample processing applied to copy-number estimation in eukaryotic cells. Nat. Methods 11: 319-324.

Kull, F. J., R. D. Vale, and R. J. Fletterick. 1998. The case for a common ancestor: kinesin and myosin motor proteins and G proteins. J. Muscle Res. Cell Motil. 19: 877-886.

Larsen, R. A., C. Cusumano, A. Fujioka, G. Lim-Fong, P. Patterson, and J. Pogliano. 2007. Treadmilling of a prokaryotic tubulin-like protein, TubZ, required for plasmid stability in *Bacillus thuringiensis*. Genes Dev. 21: 1340-1352.

Lassak, K., T. Neiner, A. Ghosh, A. Klingl, R. Wirth, and S. V. Albers. 2012. Molecular analysis of the crenarchaeal flagellum. Mol. Microbiol. 83: 110-124.

Lawrence, C. J., R. K. Dawe, K. R. Christie, D. W. Cleveland, S. C. Dawson, S. A. Endow, L. S. B. Goldstein, H. V. Goodson, N. Hirokawa, J. Howard, et al. 2004. A standardized kinesin nomenclature. J. Cell Biol. 167: 19-22.

Li, G. W., D. Burkhardt, C. Gross, and J. S. Weissman. 2014. Quantifying absolute protein synthesis rates reveals principles underlying allocation of cellular resources. Cell 157: 624635.

Lindås, A. C., E. A. Karlsson, M. T. Lindgren, T. J. Ettema, and R. Bernander. 2008. A unique cell division machinery in the Archaea. Proc. Natl. Acad. Sci. USA 105: 18942-18946.

Liu, R., and H. Ochman. 2007. Stepwise formation of the bacterial flagellar system. Proc. Natl. Acad. Sci. USA 104: 7116-7121.

Lleo, M. M., P. Canepari, and G. Satta. 1990. Bacterial cell shape regulation: testing of additional predictions unique to the two-competing-sites model for peptidoglycan assembly and isolation of conditional rod-shaped mutants from some wild-type cocci. J. Bacteriol. 172: 3758-3771.

Lovely, P. S., and F. W. Dahlquist. 1975. Statistical measures of bacterial motility and chemotaxis. J. Theor. Biol. 50: 477-496.

Löwe, J., and L. A. Amos. 2009. Evolution of cytomotive filaments: the cytoskeleton from prokaryotes to eukaryotes. Int. J. Biochem. Cell Biol. 41: 323-329.

Lu, P., C. Vogel, R. Wang, X. Yao, and E. M. Marcotte. 2007. Absolute protein expression profiling estimates the relative contributions of transcriptional and translational regulation. Nat. Biotechnol. 25: 117-124.

Ludington, W. B., L. Z. Shi, Q. Zhu, M. W. Berns, and W. F. Marshall. 2012. Organelle size equalization by a constitutive process. Curr. Biol. 22: 2173-2179.

Ludington, W. B., K. A. Wemmer, K. F. Lechtreck, G. B. Witman, and W. F. Marshall. 2013. Avalanche-like behavior in ciliary import. Proc. Natl. Acad. Sci. USA 110: 3925-3930.

Lynch, M., and G. K. Marinov. 2015. The bioenergetic costs of a gene. Proc. Natl. Acad. Sci. USA 112: 15690-15695.

Lynch, M., and B. Trickovic. 2020. A theoretical framework for evolutionary cell biology. J. Mol. Biol. 432: 1861-1879.

Maezawa, K., S. Shigenobu, H. Taniguchi, T. Kubo, S. Aizawa, and M. Morioka. 2006. Hundreds of flagellar basal bodies cover the cell surface of the endosymbiotic bacterium *Buchnera aphidicola* sp. strain APS. J. Bacteriol. 188: 6539-6543.

Makarova, K. S., N. Yutin, S. D. Bell, and E. V. Koonin. 2010. Evolution of diverse cell division and vesicle formation systems in Archaea. Nat. Rev. Microbiol. 8: 731-741.

Männik, J., R. Driessen, P. Galajda, J. E. Keymer, and C. Dekker. 2009. Bacterial growth and motility in sub-micron constrictions. Proc. Natl. Acad. Sci. USA 106: 14861-14866.

Manson, M. D., P. M. Tedesco, and H. C. Berg. 1980. Energetics of flagellar rotation in bacteria. J. Mol. Biol. 138: 541-561.

Manson, M. D., P. Tedesco, H. C. Berg, F. M. Harold, and C. Van der Drift. 1977. A proton motive force drives bacterial flagella. Proc. Natl. Acad. Sci. USA 74: 3060-3064.

Margolin, W. 2009. Sculpting the bacterial cell. Curr. Biol. 19: R812-R822.

Marguerat, S., A. Schmidt, S. Codlin, W. Chen, R. Aebersold, and J. Bähler. 2012. Quantitative analysis of fission yeast transcriptomes and proteomes in proliferating and quiescent cells. Cell 151: 671-683.

Marshall, W. F. 2011. Origins of cellular geometry. BMC Biol. 9: 57.

Marshall, W. F., and J. L. Rosenbaum. 2001. Intraflagellar transport balances continuous turnover of outer doublet microtubules: implications for flagellar length control. J. Cell Biol. 155: 405-414.

Mast, F. D., R. A. Rachubinski, and J. B. Dacks. 2012. Emergent complexity in myosin V-based organelle inheritance. Mol. Biol. Evol. 29: 975-984.

McInally, S. G., J. Kondev, and S. C. Dawson. 2019. Length-dependent disassembly maintains four different flagellar lengths in *Giardia*. eLife 8: e48694.

McKean, P. G., S. Vaughan, and K. Gull. 2001. The extended tubulin superfamily. J. Cell Sci. 114: 2723-2733.

Meister, M., G. Lowe, and H. C. Berg. 1987. The proton flux through the bacterial flagellar motor. Cell 49: 643-650.

Michel, G., T. Tonon, D. Scornet, J. M. Cock, and B. Kloareg. 2010. The cell wall polysaccharide metabolism of the brown alga *Ectocarpus siliculosus*. Insights into the evolution of extracellular matrix polysaccharides in Eukaryotes. New Phytol. 188: 82-97.

Michie, K. A., and J. Löwe. 2006. Dynamic filaments of the bacterial cytoskeleton. Annu. Rev. Biochem. 75: 467-492.

Mitchell, J. G. 1991. The influence of cell size on marine bacterial motility and energetics. Microbial Ecol. 22: 227-238.

Mitchison, T., and M. Kirschner. 1984. Dynamic instability of microtubule growth. Nature 312: 237-242.

Miyata, M., R. C. Robinson, T. Q. P. Uyeda, Y. Fukumori, S.-I. Fukushim, S. Haruta, M. Homma, K. Inaba, M. Ito, C. Kaito, et al. 2020. Tree of motility – a proposed history of motility systems

in the tree of life. Genes Cells 25: 6-21.

Mogilner, A., and G. Oster. 1996. Cell motility driven by actin polymerization. Biophys. J. 71: 3030-3045.

Monds, R. D., T. K. Lee, A. Colavin, T. Ursell, S. Quan, T. F. Cooper, and K. C. Huang. 2014. Systematic perturbation of cytoskeletal function reveals a linear scaling relationship between cell geometry and fitness. Cell Rep. 9: 1528-1537.

Moon, K. H., X. Zhao, A. Manne, J. Wang, Z. Yu, J. Liu, and M. A. Motaleb. 2016. Spirochetes flagellar collar protein FlbB has astounding effects in orientation of periplasmic flagella, bacterial shape, motility, and assembly of motors in *Borrelia burgdorferi.* Mol. Microbiol. 102: 336-348.

Muthukrishnan, G., Y. Zhang, S. Shastry, and W. O. Hancock. 2009. The processivity of kinesin-2 motors suggests diminished front-head gating. Curr. Biol. 19: 442-447.

Nan, B., and D. R. Zusman. 2016. Novel mechanisms power bacterial gliding motility. Mol. Microbiol. 101: 186-193.

Neidhardt, F. C., J. L. Ingraham, and M. Schaechter. 1990. Physiology of the bacterial cell: a molecular approach. Sinauer Assoc., Inc., Sunderland, MA.

Nevers, Y., M. K. Prasad, L. Poidevin, K. Chennen, A. Allot, A. Kress, R. Ripp, J. D. Thompson, H. Dollfus, O. Poch, and O. Lecompte. 2017. Insights into ciliary genes and evolution from multi-level phylogenetic profiling. Mol. Biol. Evol. 34: 2016-2034.

Niklas, K. J. 2004. The cell walls that bind the Tree of Life. BioScience 54: 831-841.

Norbeck, J., and A. Blomberg. 1997. Two-dimensional electrophoretic separation of yeast proteins using a non-linear wide range (pH 3-10) immobilized pH gradient in the first dimension; reproducibility and evidence for isoelectric focusing of alkaline (pI $>$ 7) proteins. Yeast 13: 1519-1534.

Noselli, G., A. Beran, M. Arroyo, and A. DeSimone. 2019. Swimming *Euglena* respond to confinement with a behavioral change enabling effective crawling. Nature Phys. 15: 496-502.

Oger, P. M., and A. Cario. 2013. Adaptation of the membrane in Archaea. Biophys. Chem. 183: 42-56.

Ojkic, N., D. Serbanescu, and S. Banerjee. 2019. Surface-to-volume scaling and aspect ratio preservation in rod-shaped bacteria. eLife 8: e47033.

Okuda, K. 2002. Structure and phylogeny of cell coverings. J. Plant Res. 115: 283-288.

Osawa, M., and H. P. Erickson. 2006. FtsZ from divergent foreign bacteria can function for cell division in *Escherichia coli.* J. Bacteriol. 188: 7132-7140.

Ouzounov, N., J. P. Nguyen, B. P. Bratton, D. Jacobowitz, Z. Gitai, and J. W. Shaevitz. 2016. MreB orientation correlates with cell diameter in *Escherichia coli.* Biophys. J. 111: 1035-1043.

Ozyamak, E., J. M. Kollman, and A. Komeili. 2013. Bacterial actins and their diversity. Biochemistry 52: 6928-6939.

Pallen, M. J., and N. J. Matzke. 2006. From The Origin of Species to the origin of bacterial flagella. Nat. Rev. Microbiol. 4: 784-790.

Pallen, M. J., C. W. Penn, and R. R. Chaudhuri. 2005. Bacterial flagellar diversity in the post-genomic era. Trends Microbiol. 13: 143-149.

Pančić, M., R. R. Torres, R. Almeda, and T. Kiørboe. 2019. Silicified cell walls as a defensive trait in diatoms. Proc. Biol. Sci. 286: 20190184.

Pazour, G. J., N. Agrin, J. Leszyk, and G. B. Witman. 2005. Proteomic analysis of a eukaryotic cilium. J. Cell. Biol. 170: 103-113.

Pelve, E. A., A. C. Lindås, W. Martens-Habbena, J. R. de la Torre, D. A. Stahl, and R. Bernander. 2011. Cdv-based cell division and cell cycle organization in the thaumarchaeon *Nitrosopumilus maritimus*. Mol. Microbiol. 82: 555-566.

Pérez-Núñez, D., R. Briandet, B. David, C. Gautier, P. Renault, B. Hallet, P. Hols, R. Carballido-López, and E. Guédon. 2011. A new morphogenesis pathway in bacteria: unbalanced activity of cell wall synthesis machineries leads to coccus-to-rod transition and filamentation in ovococci. Mol. Microbiol. 79: 759-771.

Perrin, F. 1934. Mouvement Brownien d'un ellipsoide. I. Dispersion dilectrique pour des molécules ellipsoidales. J. Phys. Radium 5: 497-511.

Perrin, F. 1936. Mouvement Brownien d'un ellipsoide. II. Rotation libre et dépolarisation des fluorescences. Translation et diffusion de molécules ellipsoidales. J. Phys. Radium 7: 1-11.

Pilhofer, M., M. S. Ladinsky, A. W. McDowall, G. Petroni, and G. J. Jensen. 2011. Microtubules in bacteria: ancient tubulins build a five-protofilament homolog of the eukaryotic cytoskeleton. PLoS Biol. 9: e1001213.

Pirie, N. W. 1973. On being the right size. Annu. Rev. Microbiol. 27: 119-132.

Pla, J., M. Sanchez, P. Palacios, M. Vicente, and M. Aldea. 1991. Preferential cytoplasmic location of FtsZ, a protein essential for *Escherichia coli* septation. Mol. Microbiol. 5: 1681-1686.

Preisner, H., J. Habicht, S. G. Garg, and S. B. Gould. 2018. Intermediate filament protein evolution and protists. Cytoskeleton 75: 231-243.

Preston, T. M., and C. A. King. 2003. Locomotion and phenotypic transformation of the amoeboflagellate *Naegleria gruberi* at the water-air interface. J. Eukaryot. Microbiol. 50: 245-251.

Prostak, S. M., K. A. Robinson, M. A. Titus, and L. K. Fritz-Laylin. 2021. The actin networks of chytrid fungi reveal evolutionary loss of cytoskeletal complexity in the fungal kingdom. Curr. Biol. 31: 1192-1205.

Purcell, E. M. 1977. Life at low Reynolds number. Amer. J. Physics 45: 3-11.

Quintero, O. A., and C. M. Yengo. 2012. Myosin X dimerization and its impact on cellular functions. Proc. Natl. Acad. Sci. USA 109: 17313-17314.

Raven, J. A. 1982. The energetics of freshwater algae; energy requirements for biosynthesis and volume regulation. New Phytol. 92: 1-20.

Raven, J. A. 1983. The transport and function of silicon in plants. Biol. Rev. 58: 179-207.

Raven, J. A., and K. Richardson. 1984. Dinophyte flagella: a cost-benefit analysis. New Phytol. 98: 259-276

Richards, T. A., and T. Cavalier-Smith. 2005. Myosin domain evolution and the primary divergence of eukaryotes. Nature 436: 1113-1118.

Rosenbaum, J. L., and G. B. Witman. 2002. Intraflagellar transport. Nat. Rev. Mol. Cell Biol. 3: 813-825.

Ross, L., and B. B. Normark. 2015. Evolutionary problems in centrosome and centriole biology. J. Evol. Biol. 28: 995-1004.

Rossmann, F. M., and M. Beeby. 2018. Insights into the evolution of bacterial flagellar motors from high-throughput *in situ* electron cryotomography and subtomogram averaging. Acta Crystallogr. D Struct. Biol. 74: 585-594.

Rueda, S., M. Vicente, and J. Mingorance. 2003. Concentration and assembly of the division ring proteins FtsZ, FtsA, and ZipA during the *Escherichia coli* cell cycle. J. Bacteriol. 185: 3344-3351.

Salje, J., P. Gayathri, and J. Löwe. 2010. The ParMRC system: molecular mechanisms of plasmid segregation by actin-like filaments. Nat. Rev. Microbiol. 8: 683-692.

Samson, R. Y., and S. D. Bell. 2009. Ancient ESCRTs and the evolution of binary fission. Trends Microbiol. 17: 507-513.

Satir, P., C. Guerra, and A. J. Bell. 2007. Evolution and persistence of the cilium. Cell Motil. Cytoskeleton 64: 906-913.

Sato, K., Y. Watanuki, A. Takahashi, P. J. O. Miller, H. Tanaka, R. Kawabe, P. J. Ponganis, Y. Handrich, T. Akamatsu, Y. Watanabe, et al. 2007. Stroke frequency, but not swimming speed, is related to body size in free-ranging seabirds, pinnipeds and cetaceans. Proc. Biol. Sci. 274: 471-477.

Saxena, I. M., and R. M. Brown, Jr. 2005. Cellulose biosynthesis: current views and evolving concepts. Ann. Bot. 96: 9-21.

Schavemaker, P. E., and M. Lynch. 2022. Flagellar energy costs across the Tree of Life. eLife 11: e77266.

Scholey, J. M. 2013. Kinesin-2: a family of heterotrimeric and homodimeric motors with diverse intracellular transport functions. Annu. Rev. Cell Dev. Biol. 29: 443-469.

Schwanhäusser, B., D. Busse, N. Li, G. Dittmar, J. Schuchhardt, J. Wolf, W. Chen, and M. Selbach. 2011. Global quantification of mammalian gene expression control. Nature 473: 337-342.

Sehring, I. M., C. Reiner, J. Mansfeld, H. Plattner, and R. Kissmehl. 2007. A broad spectrum of actin paralogs in *Paramecium tetraurelia* cells display differential localization and function. J. Cell Sci. 120: 177-190.

Seidler, R. J., and M. P. Starr. 1968. Structure of the flagellum of *Bdellovibrio bacteriovorus.* J. Bacteriol. 95: 1952-1955.

Shastry, S., and W. O. Hancock. 2010. Neck linker length determines the degree of processivity in kinesin-1 and kinesin-2 motors. Curr. Biol. 20: 939-943.

Schuech, R., T. Hoehfurtner, D. J. Smith, and S. Humphries. 2019. Motile curved bacteria are Pareto-optimal. Proc. Natl. Acad. Sci. USA 116: 14440-14447.

Siefert, J. L., and G. E. Fox. 1998. Phylogenetic mapping of bacterial morphology. Microbiology 144: 2803-2808.

Smith, J. C., J. G. Northey, J. Garg, R. E. Pearlman, and K. W. Siu. 2005. Robust method for proteome analysis by MS/MS using an entire translated genome: demonstration on the ciliome of *Tetrahymena thermophila.* J. Proteome Res. 4: 909-919.

Sosinsky, G. E., N. R. Francis, D. J. DeRosier, J. S. Wall, M. N. Simon, and J. Hainfeld. 1992. Mass determination and estimation of subunit stoichiometry of the bacterial hook-basal body flagellar complex of *Salmonella typhimurium* by scanning transmission electron microscopy. Proc. Natl. Acad. Sci. USA 89: 4801-4805.

Steenbakkers, P. J., W. J. Geerts, N. A. Ayman-Oz, and J. T. Keltjens. 2006. Identification of pseudomurein cell wall binding domains. Mol. Microbiol. 62: 1618-1630.

Stepanek, L., and G. Pigino. 2016. Microtubule doublets are double-track railways for intraflagellar transport trains. Science 352: 721-724.

Snyder, L. A., N. J. Loman, K. Fütterer, and M. J. Pallen. 2009. Bacterial flagellar diversity and evolution: seek simplicity and distrust it? Trends Microbiol. 17: 1-5.

Sweeney, H. L., and E. L. F. Holzbaur. 2016. Motor proteins, Pages 69-86. In T. D. Pollard and R. D. Goldman (eds.) The Cytoskeleton. Cold Spring Harbor Laboratory Press, Cold Spring Harbor, NY.

Szewczak-Harris, A., and J. Löwe. 2018. Cryo-EM reconstruction of AlfA from *Bacillus subtilis* reveals the structure of a simplified actin-like filament at 3.4-Å resolution. Proc. Natl. Acad. Sci. USA 115: 3458-3463.

Tam, L. W., W. L. Dentler, and P. A. Lefebvre. 2003. Defective flagellar assembly and length regulation in LF3 null mutants in *Chlamydomonas.* J. Cell Biol. 163: 597-607.

Tam, D., and A. E. Hosoi. 2011. Optimal feeding and swimming gaits of biflagellated organisms. Proc. Natl. Acad. Sci. USA 108: 1001-1006.

Tamames, J., M. Gonzalez-Moreno, J. Mingorance, A. Valencia, and M. Vicente. 2001. Bringing gene order into bacterial shape. Trends Genet. 17: 124-126.

Taniguchi, Y., P. J. Choi, G. W. Li, H. Chen, M. Babu, J. Hearn, A. Emili, and X. S. Xie. 2010. Quantifying *E. coli* proteome and transcriptome with single-molecule sensitivity in single cells. Science 329: 533-538.

Taylor, T. B., G. Mulley, A. H. Dills, A. S. Alsohim, L. J. McGuffin, D. J. Studholme, M. W. Silby, M. A. Brockhurst, L. J. Johnson, and R. W. Jackson. 2015. Evolutionary resurrection of flagellar motility via rewiring of the nitrogen regulation system. Science 347: 1014-1017.

Tchoufag, J., P. Ghosh, C. B. Pogue, B. Nan, and K. K. Mandadapu. 2019. Mechanisms for bacterial gliding motility on soft substrates. Proc. Natl. Acad. Sci. USA 116: 25087-25096.

Thomas, N. A., S. L. Bardy, and K. F. Jarrell. 2001. The archaeal flagellum: a different kind of prokaryotic motility structure. FEMS Microbiol. Rev. 25: 147-174.

Titus, M. A. 2016. Myosin-driven intracellular transport, Pages 265-279. In T. D. Pollard and R. D. Goldman (eds.) The Cytoskeleton. Cold Spring Harbor Laboratory Press, Cold Spring Harbor, NY.

Tocheva, E. I., E. G. Matson, D. M. Morris, F. Moussavi, J. R. Leadbetter, and G. J. Jensen. 2011. Peptidoglycan remodeling and conversion of an inner membrane into an outer membrane during sporulation. Cell 146: 799-812.

Tocheva, E. I., D. R. Ortega, and G. J. Jensen. 2016. Sporulation, bacterial cell envelopes and the origin of life. Nat. Rev. Microbiol. 14: 535-542.

Toft, C., and M. A. Fares. 2008. The evolution of the flagellar assembly pathway in endosymbiotic

bacterial genomes. Mol. Biol. Evol. 25: 2069-2076.

Turner, L., W. S. Ryu, and H. C. Berg. 2000. Real-time imaging of fluorescent flagellar filaments. J. Bacteriol. 182: 2793-2801.

Typas, A., M. Banzhaf, C. A. Gross, and W. Vollmer. 2011. From the regulation of peptidoglycan synthesis to bacterial growth and morphology. Nat. Rev. Microbiol. 10: 123-136.

Ursell, T. S., J. Nguyen, R. D. Monds, A. Colavin, G. Billings, N. Ouzounov, Z. Gitai, J. W. Shaevitz, and K. C. Huang. 2014. Rod-like bacterial shape is maintained by feedback between cell curvature and cytoskeletal localization. Proc. Natl. Acad. Sci. USA 111: E1025-E1034.

van Dam, T. J., M. J. Townsend, M. Turk, A. Schlessinger, A. Sali, M. C. Field, and M. A. Huynen. 2013. Evolution of modular intraflagellar transport from a coatomer-like progenitor. Proc. Natl. Acad. Sci. USA 110: 6943-6948.

Van Niftrik, L., W. J. C. Geerts, E. G. van Donselaar, B. M. Humbel, R. I. Webb, H. R. Harhangi, H. J. M. Op den Camp, J. A. Fuerst, A. J. Verkleij, M. S. M. Jetten, and M. Strous. 2009. Cell division ring, a new cell division protein and vertical inheritance of a bacterial organelle in anammox planctomycetes. Mol. Microbiol. 73: 1009-1019.

Velle, K. B., and L. K. Fritz-Laylin. 2019. Diversity and evolution of actin-dependent phenotypes. Curr. Opin. Genet. Dev. 58/59: 40-48.

Veltman, D. M., and R. H. Insall. 2010. WASP family proteins: their evolution and its physiological implications. Mol. Biol. Cell 21: 2880-2893.

Veyrier, F. J., N. Biais, P. Morales, N. Belkacem, C. Guilhen, S. Ranjeva, O. Sismeiro, G. Péhau-Arnaudet, E. P. Rocha, C. Werts, et al. 2015. Common cell shape evolution of two nasopharyngeal pathogens. PLoS Genet. 11: e1005338.

Vischer, N. O., J. Verheul, M. Postma, B. van den Berg van Saparoea, E. Galli, P. Natale, K. Gerdes, J. Luirink, W. Vollmer, M. Vicente, T. den Blaauwen, et al. 2015. Cell age dependent concentration of *Escherichia coli* divisome proteins analyzed with ImageJ and ObjectJ. Front. Microbiol. 6: 586.

Visweswaran, G. R., B. W. Dijkstra, and J. Kok. 2011. Murein and pseudomurein cell wall binding domains of bacteria and archaea – a comparative view. Appl. Microbiol. Biotechnol. 92: 921-928.

Vollmer, W. 2011. Bacterial outer membrane evolution via sporulation? Nat. Chem. Biol. 8: 14-18.

Vollmer, W., and S. J. Seligman. 2010. Architecture of peptidoglycan: more data and more models. Trends Microbiol. 18: 59-66.

Wadhams, G. H., and J. P. Armitage. 2004. Making sense of it all: bacterial chemotaxis. Nat. Rev. Mol. Cell Biol. 5: 1024-1037.

Wadhwa, N., and H. C. Berg. 2022. Bacterial motility: machinery and mechanisms. Nat. Rev. Microbiol. 20: 161-173.

Wagstaff, J., and J. Löwe. 2018. Prokaryotic cytoskeletons: protein filaments organizing small cells. Nat. Rev. Microbiol. 16: 187-201.

Walter, W. J., and S. Diez. 2012. Molecular motors: a staggering giant. Nature 482: 44-45.

Walsby, A. E. 1994. Gas vesicles. Microbiol. Rev. 58: 94-144.

Wang, S., L. Furchtgott, K. C. Huang, and J. W. Shaevitz. 2012. Helical insertion of peptidoglycan produces chiral ordering of the bacterial cell wall. Proc. Natl. Acad. Sci. USA 109: E595-E604.

Waterbury, J. B., J. M. Willey, D. G. Franks, F. W. Valois, and S. W. Watson. 1985. A cyanobacterium capable of swimming motility. Science 230: 74-76.

Wickstead, B., and K. Gull. 2007. Dyneins across eukaryotes: a comparative genomic analysis. Traffic 8: 1708-1721.

Wickstead, B., and K. Gull. 2011. The evolution of the cytoskeleton. J. Cell Biol. 194: 513-525.

Wickstead, B., K. Gull, and T. A. Richards. 2010. Patterns of kinesin evolution reveal a complex ancestral eukaryote with a multifunctional cytoskeleton. BMC Evol. Biol. 10: 110.

Wientjes, F. B., C. L. Woldringh, and N. Nanninga. 1991. Amount of peptidoglycan in cell walls of gram-negative bacteria. J. Bacteriol. 173: 7684-7691.

Wilkes, D. E., H. E. Watson, D. R. Mitchell, and D. J. Asai. 2008. Twenty-five dyneins in *Tetrahymena:* a re-examination of the multidynein hypothesis. Cell Motil. Cytoskeleton 65: 342-351.

Wiśniewski, J. R., and D. Rakus. 2014. Quantitative analysis of the *Escherichia coli* proteome. Data Brief 1: 7-11.

Wu, J. Q., and T. D. Pollard. 2005. Counting cytokinesis proteins globally and locally in fission yeast. Science 310: 310-314.

Yin, Q. Y., P. W. de Groot, L. de Jong, F. M. Klis, and C. G. De Koster. 2007. Mass spectrometric quantitation of covalently bound cell wall proteins in *Saccharomyces cerevisiae.* FEMS Yeast Res. 7: 887-896.

Young, K. D. 2006. The selective value of bacterial shape. Microbiol. Mol. Biol. Rev. 70: 660-703.

Young, K. D. 2010. Bacterial shape: two-dimensional questions and possibilities. Annu. Rev. Microbiol. 64: 223-240.

Zhang, P., W. Dai, J. Hahn, and S. P. Gilbert. 2015. *Drosophila* Ncd reveals an evolutionarily conserved powerstroke mechanism for homodimeric and heterodimeric kinesin-14s. Proc. Natl. Acad. Sci. USA 112: 6359-6364.

Zhu, S., T. Nishikino, B. Hu, S. Kojima, M. Homma, and J. Liu. 2017. Molecular architecture of the sheathed polar flagellum in *Vibrio alginolyticus.* Proc. Natl. Acad. Sci. USA 114: 10966-10971.

Figure 16.1. Examples of the structural forms derived from the three key forms of fibril-forming proteins in eukaryotes. Individual tubulin filaments are comprised of heterodimers of two elemental forms of tubulin (purple and blue). Intermediate filaments can assemble into higher-order structures such as cables and sheets.

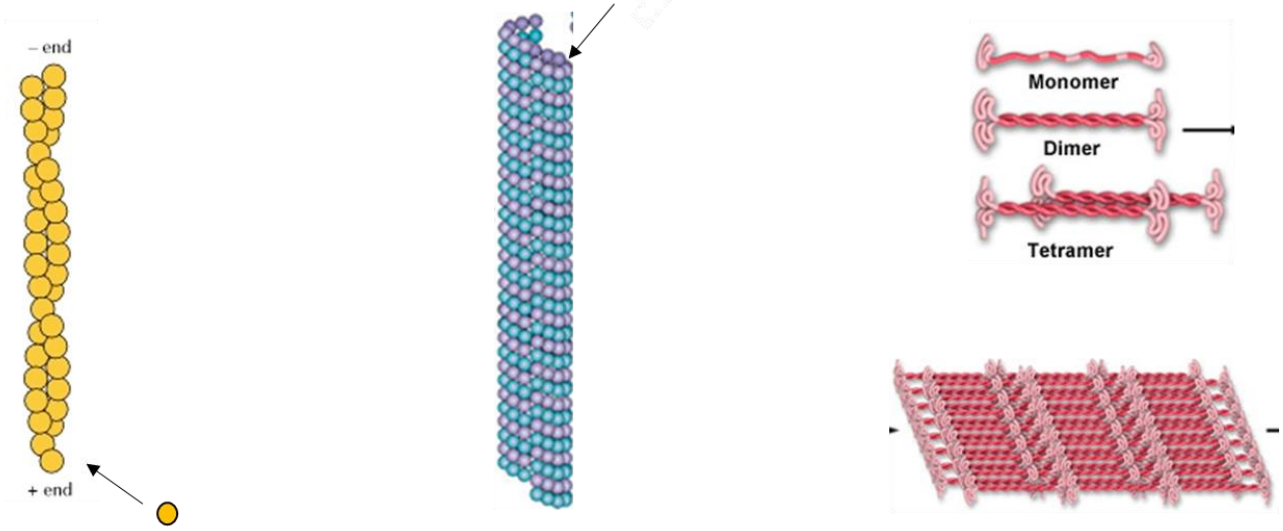

Actin Tubulin Intermediate Filaments

Figure 16.2. A cartoon version of a peptidoglycan layer. The paired hexagons represent dimers of NAM and NAG, whereas the small chains represent cross-linked peptides.

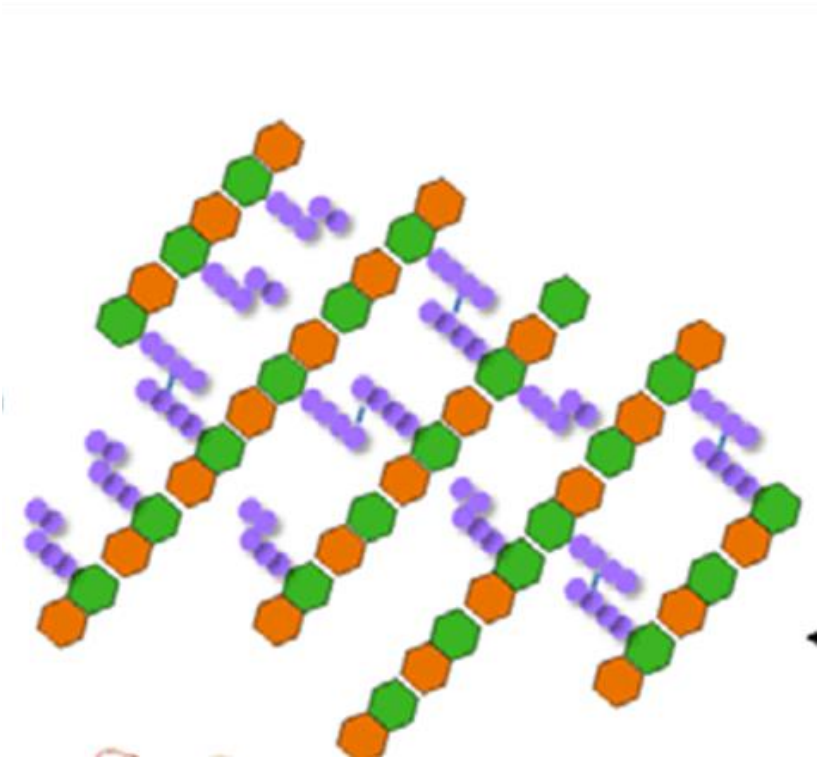

Figure 16.3. An example of a motor protein interfacing with a microtubule, along which it walks fueled by energy derived from ATP hydrolysis, carrying its cargo (in this case a transport vesicle).

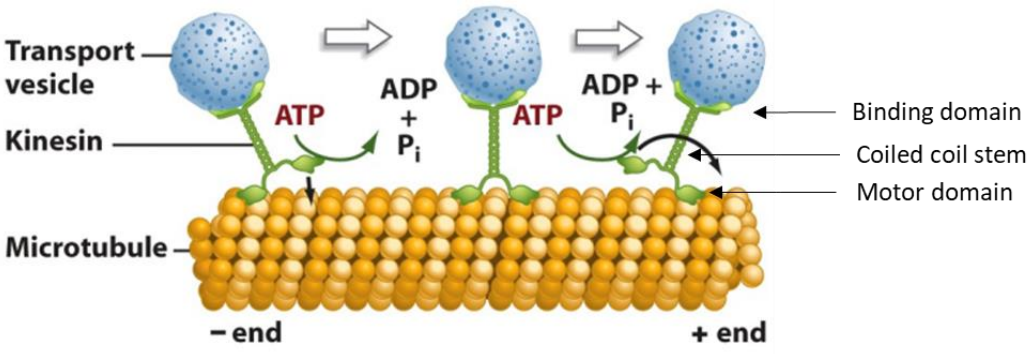

Figure 16.4. Idealized schematics of bacterial (left) and eukaryotic (right) flagella. The former emanates from a complex apparatus embedded in the double membrane, and operates in a corksrew-like manner. The latter grows out of a basal body (centriole), has an interior consisting of tubulins along which motor proteins move (not shown), and operates in a whip-like manner.

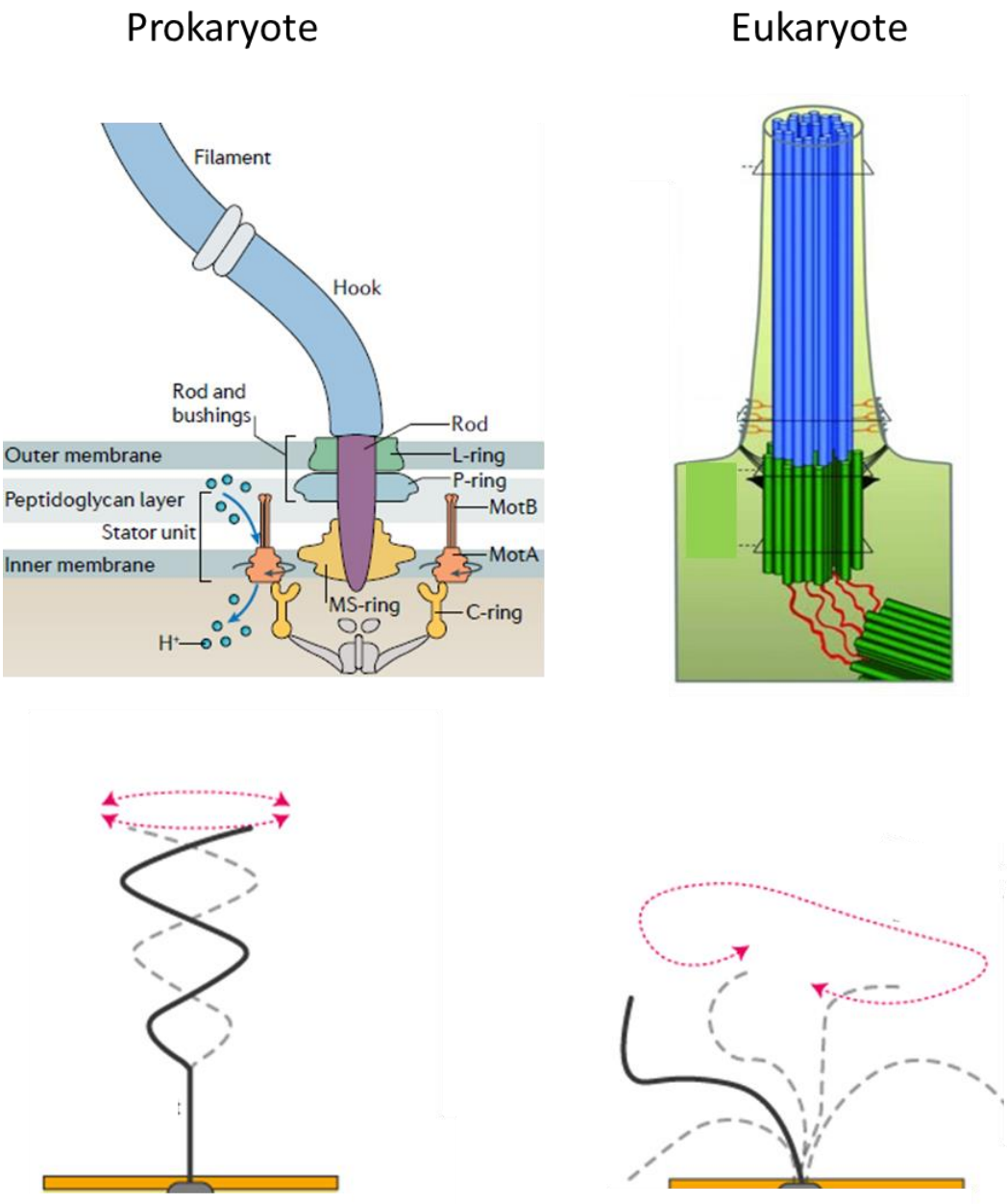

Figure 16.5. Scaling relationships for swimming speeds and flagellar construction costs with respect to cell volume. **a)** Swimming speeds (v) and cell volume (V) in unicellular species. For eukaryotes, $v = 16.6V^{0.25}$, $r^2 = 0.35$); and for bacteria, $v = 29.5V^{0.17}$, $r^2 = 0.17$) (as the data are very noisy, the data for all phylogenetic groups were pooled for the eukaryote analysis). The measured values are corrected for temperature assuming a Q_{10} of 2.5. From Lynch and Trickovic (2020). **b)** Absolute costs of total flagellar construction. In units of 10^9 ATP hydrolyses, the fitted power-law relationships are: $1.1V^{0.81}$ for bacteria, $2.6V^{0.31}$ for eukaryotic flagellates excluding ciliates and parabasalids, which are described by $2.8V^{0.86}$. **c** Flagellar construction costs as a fraction of total-cell construction costs. **d)** Swimming speed (in units of cell length) per ATP invested in flagellar construction. In units of 10^{-8}, the regressions for bacteria and eukaryotes are, respectively, $2.7V^{-1.13}$ and $3.1V^{-1.06}$. The data for the final three panels are taken from Schavemaker and Lynch (2022).